1-1-1982

Fracture initiation in weldments with or without crack-like imperfections.

Erdogan Madenci

FRACTURE INITIATION IN WELDMENTS WITH OR WITHOUT CRACK-LIKE IMPERFECTIONS

by

Erdogan Madenci

A Thesis

Presented to the Graduate Committee

of Lehigh University

in Candidacy for the Degree of

Master of Science

in

Applied Mechanics

Lehigh University

1982

This thesis is accepted and approved in partial fulfillment of the requirement for the degree of Master of Science.

April 27, 1982
(date)

George C. Sih
Professor in Charge

Chairman of Department

ACKNOWLEDGEMENTS

The author wishes to express his gratitude to his advisor, Professor George C. Sih, for his stimulating ideas and the support which made this work possible.

Dr. Bruce Kiefer's knowledge of numerical methods and his helpful advice were greatly appreciated.

Thanks are also due to Mrs. Barbara DeLazaro for her care and patience in the preparation of the final manuscript.

TABLE OF CONTENTS

LIST OF TABLES

LIST OF FIGURES

LIST OF FIGURES - CONTINUED

ABSTRACT

The purpose of this dissertation is to investigate the location of possible failure sites and fracture initiation in weldments with or without crack-like imperfections by application of strain energy density theory with incremental theory of plasticity. Each zone of weldments under investigation is modeled to withstand extensive amount of yielding. A finite element method is used to perform the stress analysis.

The different weld configurations are investigated with increasing severity in terms of the type of mechanical defects encountered in fabrication. The perfect joint is analyzed for reference purpose. The decreasing load carrying capacity of the welded structure is determined for a joint with a notch and a crack in the HAZ. The strain energy density criterion is applied consistently to all three weld configurations such that the loading, geometric and material parameters can be studied in a combined and consistent fashion.

CHAPTER I - INTRODUCTION

Despite the extreme precautions taken during weld fabrication, welds are frequently imperfect in that they may be misaligned or contain defects. These defects, in the form of cracks or voids, can lead to premature or unexpected failure of structures such as pressure vessels, aerospace components, etc. Weldments are prone to failure by crack propagation because:

1. A weldment provides continuity in load transfer from one component of the structure to another. Hence, crack growth can be extensive once started.

2. Welds often contain various types of defects, such as cracks, porosity and slag inclusions.

3. The interface between the base and weld material referred to as the heat-affected zone* is a weak link of the system. Thermal gradients arising from welding can introduce undesirable residual stresses and excessive geometric distortion.

A prerequisite to the application of fracture mechanics to weldments is a knowledge of the stress state during and after the

*The grain sizes within the heat-affected zone (HAZ) will vary and be different from those in the weld material (WM) and base material (BM).

welding process. Although residual stresses will prevail, they may or may not be important depending on the properties of the material and the fabrication procedure. If the welded material is ductile and cracking occurred together with appreciable deformation, then residual stresses have little or no effect on the subsequent fracture behavior of the weldment because their effects have been diminished through yielding and fracture [1]. Rewelding is not recommended [2] because it is not only an extremely costly procedure but it may further degrade the weld quality and introduce additional defects.

In order to ascertain the integrity of weldments, it is necessary to establish criteria that can assess load carrying capability of weldments so that acceptability conditions can be established. Past work in this area tended to oversimplify the problem and did not pay sufficient attention to an understanding of the combined effect of material and loading.

The function of a weldment is to transfer load, and hence it must be regarded as a composite structure. It is composed of various zones of different metallurgical properties: the weld metal (WM), the heat-affected base metal near the weld and the unaffected base metal (BM). The heat-affected zone (HAZ), although very narrow, is composed of many regions of different metallurgical structures. Because weldments undergo gross yielding and behave nonlinearly, their behaviors are inherently load history

dependent. Hence, information collected from welded tensile specimens serves little use and cannot be transferred to structure design. For this reason, many of the investigations [3,4] employing linear elastic fracture mechanics (LEFM) are obviously fundamentally unsound and their results are suspect. More specifically, the critical stress intensity factor K_{1c} or the crack opening displacement (COD) approach cannot reliably characterize the fracture behavior of weldments. Some of their limitations may be outlined as follows:

1. The K_{1c} or COD concept relies on the existence of an initial crack. Because of the nonhomogeneous material properties within a weld, it is not clear where crack initiation will first occur and hence an a priori knowledge of the location of initial cracks is required by the LEFM method.

2. Crack initiation can occur in any plane that is not necessarily aligned normal to the applied load, a condition that is required in the application of LEFM*.

*The energy release rate quantity has been applied to solve curved crack problems by necessitating the stress solution of a branched crack and performing the questionable limiting process. The approach requires cumbersome analytical work, is problematic and simply impractical.

The current concept of characterizing weldment behavior by a single parameter such as K_{1c} or critical COD is ill-conceived. A weldment is a nonhomogeneous system, and each section of the weld such as WM, HAZ and BM must be addressed separately. What should be determined is the load carrying capacity of the weld and not some ill-conceived fracture parameters that serve no useful purpose. Many of the claims made by the LEFM practitioners [5] are simply not valid.

The selection of a suitable failure criterion should not be based on force-fitting experimental data with concocted analytical theories or results. It is desirable to have a criterion that possesses versatility and ease for treating, not just a few specialized situations, but general loadings, complex geometries and different materials whether linearly elastic or nonlinearly plastic. Sih [6] proposed the Strain Energy Density (SED) criterion for characterizing the fracture behavior of ductile and brittle materials with the objective of resolving the specimen size effect [7]. Sih's theory assumes that the critical strain energy density function $(dW/dV)_c$ is a material constant that may be applied to predict fracture initiation of a material element near a crack tip, notch tip, reentrant corner, or in an unflawed structure [7].

This versatility of Sih's theory is unique because, unlike the LEFM approach, which is based on an energy release rate or stress intensity factor, it does not require a precise knowledge of the

size and location of the initial flaw. In addition, SED criterion has been valuable in predicting crack path, fracture load and crack instability for structural members subjected to mixed mode loading conditions.

The main objective of this dissertation is to apply the SED criterion for predicting failure in welded joints. Potential failure sites are identified with the help of results obtained from plasticity stress analysis, using the finite element method.

CHAPTER II - CURRENT METHODOLOGY

Ductility is a desirable feature of weldments, as it permits the dissipation of energy due to deformation and distortion, the lack of which could lead to failure. To design for ductility is difficult because weldment behavior is influenced by loading, geometry and material properties. Specimen thickness alone for example can influence the brittle to ductile transition [7], Figure 1 in which σ_c is the critical applied stress on a specimen containing a crack of length 2a. This transition region represents a change in failure mode from the very brittle by rapid crack propagation to the very ductile by plastic collapse.

Comprehensive reviews of elastic-plastic fracture can be found in [7-9]. The LEFM theory applies only for very thick specimens when the quantity $\sigma_c\sqrt{\pi a}$ no longer varies with the specimen thickness. Only then it can be referred to as the fracture toughness value K_{1c}. The K_{1c} type of specimen testing approach cannot be applied to weldments because energy release at instability, should it happen by the propagation of a single crack, can only occur in one part of material at a given time: either in WM, HAZ or BM. In other words, *fracture toughness* applies in the case of a homogeneous material.

One of the current methods for measuring the so-called material toughness of weldments is to machine a sharp notch in or near a welded joint and load it to failure. For instance, the COD bend

test or the notched tension tests are often used for this purpose. In addition to the criticisms of the basic approach as stated earlier, the test data contains much scatter. This is due to variations in notch locations, orientations, weldment and specimen design [10]. Despite these shortcomings, the COD approach is being adopted by many practitioners and researchers. Their results are inconsistent in that they themselves cannot agree on the location of the crack where the COD measurement should be taken. In fact, the COD quantity in itself has no physical meaning and its relationship with the critical stress intensity factor K_{1c} or energy release rate G_{1c} holds only if the material is linearly elastic, given by [11]:

$$G_{1c} = \text{COD}\ \sigma_{ys},\ G_{1c} = \frac{(1-\nu^2)K_{1c}^2}{E}\ \text{(plane strain)} \qquad (1)$$

where σ_{ys} is the yield strength and E is the Young's modulus. Needless to say, the above relationship cannot be applied when yielding takes place ahead of the crack [12]. Note that equation (1) renders grossly different values of G_{1c} for the two curves shown in Figure 2.

Since weldments undergo yielding at large, the COD approach cannot be expected to give accurate results. The path independent J-integral has the same basic shortcomings as it cannot account for the energy dissipated due to plastic deformation. The empirical relation

$$J = m\sigma_{ys}\ COD \tag{2}$$

is subject to the same criticisms as equation (1). The parameter m is determined experimentally. The range of $1 \leq m \leq 2$ has been claimed [13]. Although equations (1) and (2) are similar, J does not have the physical meaning of energy release rate, as G. The only difference between J and G is that the former applies to a nonlinear elastic material and the latter to a linear elastic material. Both quantities lose their significance when applied to an elastic-plastic material whose behavior depends on load history. Despite this obvious limitation, K_{Ic}, COD and J have been used indiscriminantly to welded structures [14].

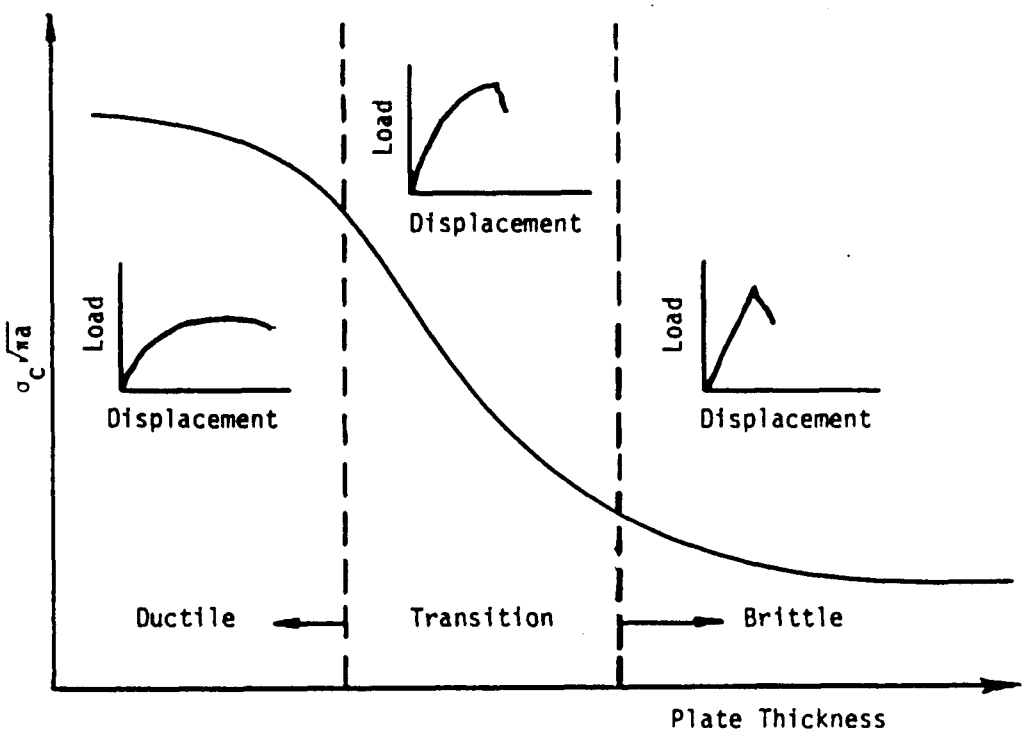

FIGURE 1 - VARIATION OF K_{Ic} WITH PLATE THICKNESS

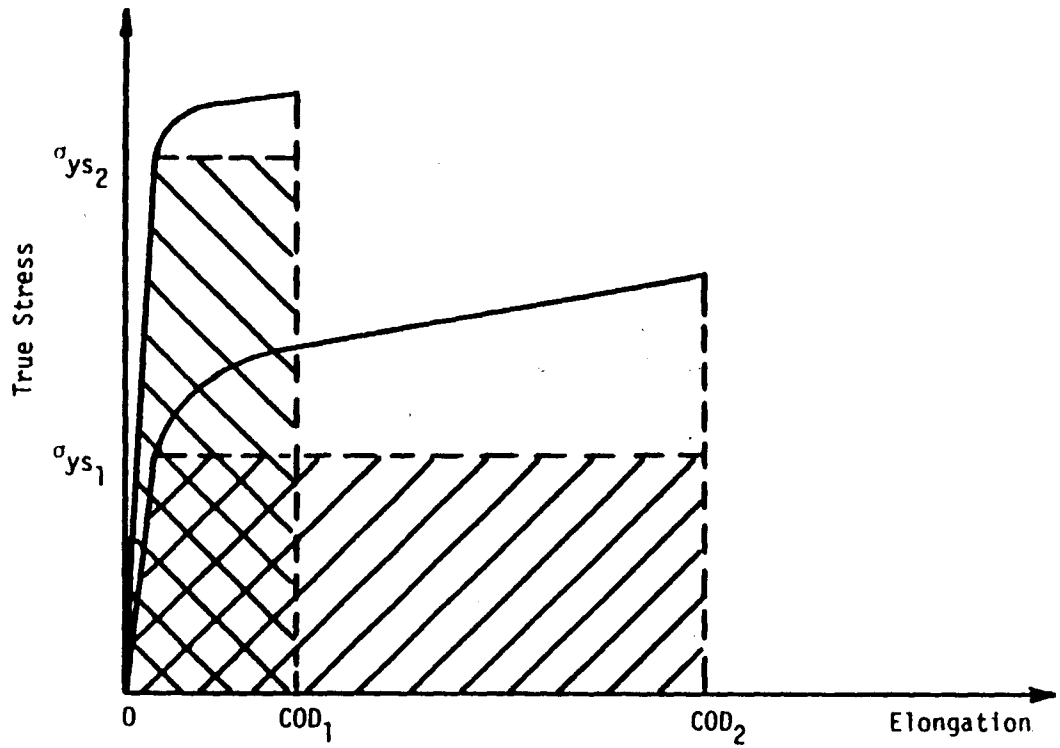

FIGURE 2 - COD VERSUS σ_{ys}

CHAPTER III - STRAIN ENERGY DENSITY THEORY

A complete description of the stress and strain state of a given element requires a knowledge of the six components of stress and strain. The prediction of failure by yielding and/or fracture requires the specification of failure criteria. The two classical criteria for predicting yielding are the total strain energy density, or Beltrami-Haigh theory, and the distortional energy, or Huber-von Mises Hencky theory. According to these theories, failure in a material by yielding occurs when the total or distortional strain energy per unit volume absorbed by the material equals the energy per unit volume stored in the material when loaded in uniaxial tension at yield. This quantity corresponds to the limiting strain energy density and is assumed to be a material constant. Extensive experiments have been carried out to measure the strain energy density quantity corresponding to failure by yielding [15]. A generalized strain energy density theory for predicting material failure by yielding and fracture has been proposed by Sih [16-18]. He associated yielding with the threshold values of the maxima of the strain energy density function dW/dV, and fracture initiation with the minima. This concept is extremely general since $(dW/dV)_{max}$ and $(dW/dV)_{min}$ are known to exist at a given point in all stressed solids regardless of the material behavior.

Because of the limitation of continuum mechanics theories, failure initiation cannot be identified precisely but must be assumed to occur over a finite region within which the microstructure

effects of the material cannot be ignored. The radius of this region is assumed to be r_o. The size of r_o has been estimated theoretically by Sih and Kipp [19] and experimentally by Theocaris [20]. In this connection,

$$\frac{dW}{dV} = \frac{S}{r} \tag{3}$$

follows naturally where S is known as the strain energy density factor whose critical value S_c is related to K_{1c} by the relation:

$$S_c = \frac{(1+\nu)(1-2\nu)}{2\pi E} K_{1c}^2 \tag{4}$$

When equation (3) is applied to the crack tip, r becomes r_o and dW/dV is the strain energy density in an element outside the circular or core region with radius r_o. Figure 3 gives a schematic representation of the relationship in equation (3) at the onset of fracture initiation, i.e., $(dW/dV)_c = S_c/r_c$. The critical ligament distance r_c is known once $(dW/dV)_c$ is determined from the area under the true stress and strain curve while S_c is found from a K_{1c} test.

In general, the function dW/dV can be computed from

$$\frac{dW}{dV} = \int_0^{\epsilon_{ij}} \sigma_{ij} d\epsilon_{ij} \quad i,j = 1,2,3 \tag{5}$$

where σ_{ij} and ϵ_{ij} are the rectangular components of the stress and strain tensor.

The basic hypotheses of the strain energy density theory may be stated as follows:

Hypothesis (1): The relative minima of dW/dV, $(dW/dV)_{min}$, and maxima, $(dW/dV)_{max}$, are assumed to coincide with the locations of fracture and yielding respectively.

Hypothesis (2): Yielding and fracture are assumed to initiate when $(dW/dV)_{max}$ and $(dW/dV)_{min}$ reach their respective critical values*.

Hypothesis (3): The rate of yielding and fracture are assumed to obey the relation

$$\left(\frac{dW}{dV}\right)_c = \frac{S_1}{r_1} = \frac{S_2}{r_2} = \text{---} = \frac{S_j}{r_j} = \text{---} = \frac{S_c}{r_c} = \text{const.} \tag{6}$$

if the process leads to unstable failure. Then

$$r_1 < r_2 < \text{---} < r_j < \text{---} < r_c \tag{7}$$

In situations where yielding and fracture come to arrest, then

$$r_1 > r_2 > \text{---} > r_j > \text{---} > r_o \tag{8}$$

*The critical strain energy density value $(dW/dV)_c$ in the elastic material should be distinguished from that in the plastic material $(dW/dV)^*_c$.

such that

$$\left(\frac{dW}{dV}\right)_c = \frac{S_o}{r_o} = \text{const.} \tag{9}$$

where r_o corresponds to the radius of the core region.

This completes the introduction of the strain energy density criterion. It is now pertinent to apply it to predict possible failure sites in weldments. To this end, a knowledge of the stress state in weld joints is required.

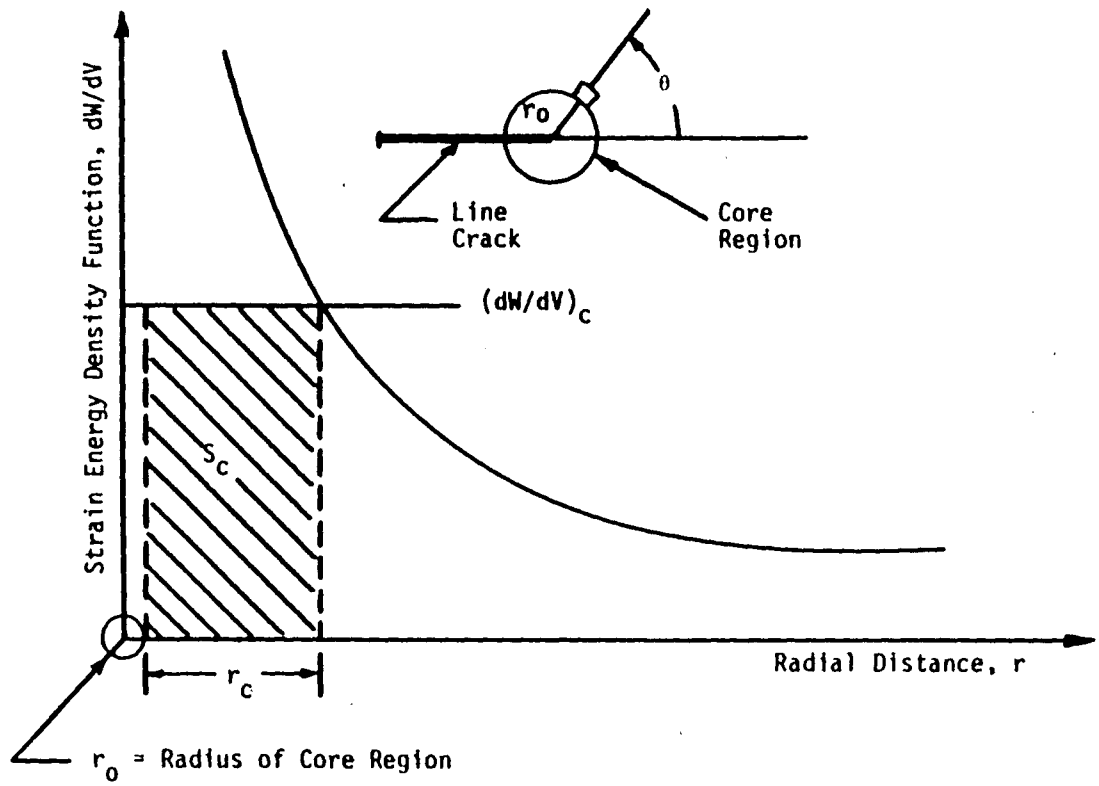

FIGURE 3 - STRAIN ENERGY DENSITY FUNCTION VERSUS RADIAL DISTANCE AHEAD OF CRACK

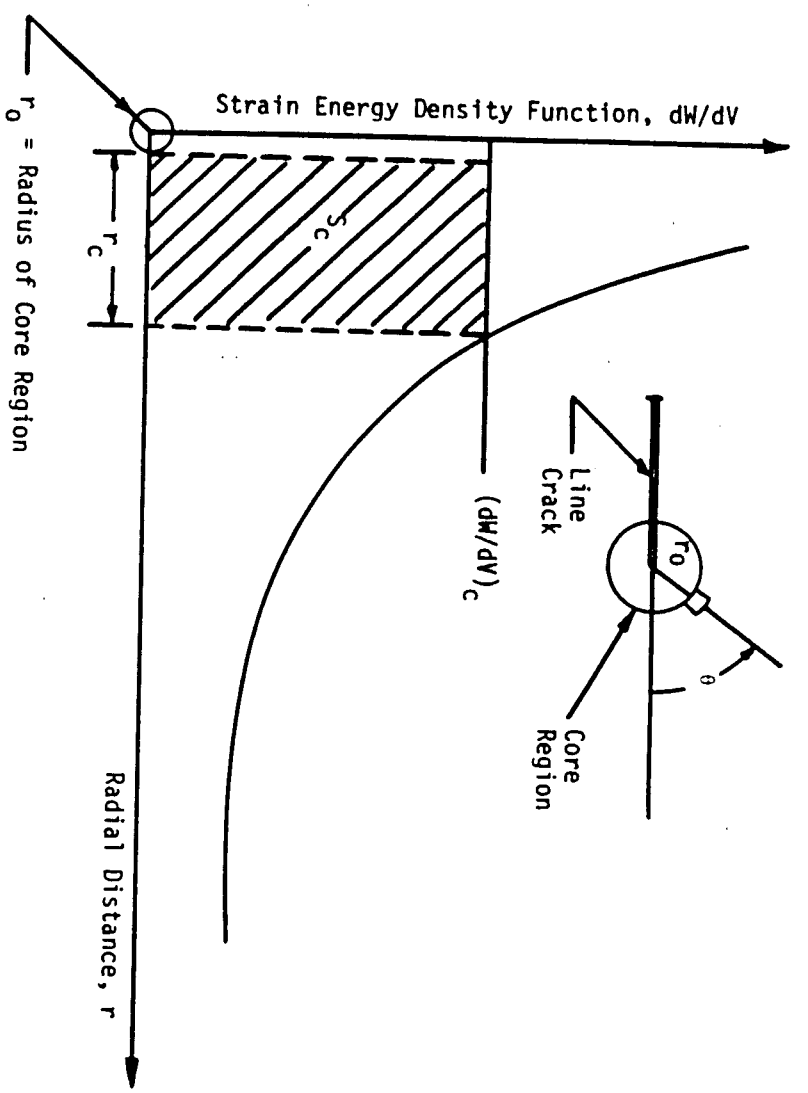

FIGURE 3 - STRAIN ENERGY DENSITY FUNCTION VERSUS RADIAL DISTANCE AHEAD OF CRACK

CHAPTER IV - STRESS ANALYSIS PROCEDURE

The stress analysis is performed using the modified version of the "Plastic Axisymmetric/Planar Structures (PAPST)" computer program that was developed to solve structural problems involving both material and geometric nonlinearities. The incremental theory of plasticity with a von Mises yield criterion is incorporated in PAPST. The twelve node quadrilateral isoparametric elements with cubic displacement shape functions are used such that accuracy near the crack is achieved by placing the two *side-nodes* at the 1/9 and 4/9 distance of the sides along the corner node at the crack tip [21]. Numerical results for the strain energy density at the nodes can vary from 10 to 20 percent depending on the interpolation technique employed. This uncertainty is avoided by displaying the values of dW/dV at the quadrature points of each element in the form of contour plots.

The effect of finite strain is incorporated in PAPST through the use of an updated Lagrangian formulation such that the coordinate system is convected with the deformation. The relationship between the true strain rate and deformation rate (or velocity) is unchanged for the small strain theory in this coordinate system. The program automatically checks and controls the equilibrium condition throughout the loading history [22].

Following the incremental variational principle presented by Washizu [23], the system under consideration refers to an arbi-

trary reference state L_R of the local path as shown in Figure 4.

It is assumed that all state variables are given at the reference state L_R upon which basis the stresses, strains and displacements of the current state L_c are determined. The current and reference state are assumed to be incrementally close. The local (initial) coordinate system X_i is taken as a Lagrangian frame of reference in relation to the current state L_c. This coordinate system is assumed to be fixed with the body as it deforms from L_R to L_c. When deformed, these coordinates also become convected. The global reference system is $\overline{X}_i$ and is used to assemble all elements of the discretized body [24], Figure 4.

Incremental plasticity equations are used. The general equilibrium equation when written in rate form in the absence of inertia effects becomes

$$\frac{\partial \dot{\sigma}_{ij}}{\partial x_j} + \dot{b}_j = 0 \tag{10}$$

in which $\dot{\sigma}_{ij}$ is the stress rate/unit volume, and $\dot{b}_j$ is the body force rate/unit volume. For incompressible plastic flow, the general constitutive equation is

$$\dot{\sigma}_{ij} = 2\mu\dot{\epsilon}_{ij} + \frac{2\mu\nu}{1-2\nu}\dot{\epsilon}_{kk}\delta_{ij} - 2\mu\dot{\epsilon}^{p}_{ij} \tag{11}$$

with μ being the shear modulus, ν the Poisson's ratio, $\dot{\epsilon}_{ij}$ the to-

tal strain rate and $\dot{\epsilon}^p_{ij}$ the plastic strain rate.

The von-Mises yield criterion or J_2-flow theory of plasticity is used. The deviatoric strain rate is expressed in terms of the current deviatoric stress components S_{ij} and the components of the deviatoric stress rate $\dot{S}_{ij}$ as follows:

$$\dot{e}_{ij} = \begin{cases} \frac{1+\nu}{E}\dot{S}_{ij} + \frac{3}{2} f(\sigma_e) S'_{ij} \dot{\sigma}'_e, \text{ where } \sigma'_e = \sigma_y;\ \dot{\sigma}'_e > 0;\ i \neq j \\ \\ \frac{1+\nu}{E}\dot{S}_{ij} \qquad\qquad\qquad\qquad \text{, otherwise} \end{cases} \tag{12}$$

in which $\dot{e}_{ij}$ is the deviatoric strain rate components,

$$\begin{aligned} \dot{e}_{ij} &= \dot{\epsilon}_{ij} - \frac{1}{3}\dot{\epsilon}_{pp}\delta_{ij} \\ S_{ij} &= \sigma_{ij} - \frac{1}{3}\sigma_{pp}\delta_{ij} \\ S'_{ij} &= S_{ij} - a_{ij} \end{aligned} \tag{13}$$

In equations (12) and (13), E is the Young's modulus, σ_y the current yield stress, S_{ij} the current deviatoric stress components, S'_{ij} the deviatoric stress components measured from the center of the current yield surface.

The coordinate a_{ij} of the stress space of the center of the yield surface is given by

$$a_{ij} = \begin{cases} \frac{3}{2}\beta S'_{k\ell}S'_{ij}/\sigma'^{2}_{e}, \text{ where } \sigma'_e=\sigma_y,\ \dot{\sigma}'_e>0 \\ \\ 0 \qquad\qquad , \text{otherwise} \end{cases} \tag{14}$$

and

$$\sigma_e = \sqrt{\frac{3}{2} S_{ij}S_{ij}} \tag{15}$$

where σ_e is the von Mises effective stress, and σ'_e the von Mises effective stress with respect to the coordinate of the current center of the yield surface:

$$\sigma'_e = \sqrt{\frac{3}{2} S'_{ij}S'_{ij}} \tag{16}$$

Let the function $f(\sigma_e)$, which depends on the uniaxial stress-strain curve, be defined as

$$f(\sigma_e) = \frac{\dot{e}^p}{\sigma_e \dot{\sigma}_e} \tag{17}$$

such that $\dot{e}^p$ represents the uniaxial plastic strain rate in terms of the effective stress and effective stress rate. The parameter β in equation (14) can vary from 0 to 1 with β=0 corresponding to isotropic hardening and β=1 to kinematic hardening. A combined isotropic and kinematic hardening can also occur. The yield surface

of isotropic hardening expands uniformly about the origin in stress space, Figure 5(a), whereas the yield surface of kinematic hardening translates as a rigid body in a direction normal to the yield surface, Figure 5(b). Combined hardening theory allows both expansion and translation of the yield surface, Figure 5(c). The derivation of the equation corresponding to these cases can be found in [25,26].

The relationship between the uniaxial stress and strain is nonlinear. Permanent deformation prevails when the material is loaded beyond the yield point. The stress-strain curve is approximated by using a multilinear model to describe the uniaxial response.

The following relationship is used:

$$\varepsilon = \frac{\sigma}{E} + \frac{\alpha_1}{E}(\sigma_1-\sigma_{ys}) + \frac{\alpha_2}{E}(\sigma_2-\sigma_1) + \text{---} + \frac{\alpha_n}{E}(\sigma_n-\sigma_{n-1}) \qquad (18)$$

where $\sigma_{n-1}<\sigma<\sigma_n$ and

$$\alpha_n = \frac{E\Delta\varepsilon_n-\Delta\sigma_n}{\Delta\sigma_n} \qquad (19)$$

The plastic strain rate is given by

$$\dot{\varepsilon}_{plastic} = \frac{\alpha_n\dot{\sigma}_e}{E} \qquad (20)$$

and hence together with equation (17), $f(\sigma_c)$ becomes

$$f(\sigma_e) = \frac{\dot{\epsilon}_{plastic}}{\dot{\sigma}_e \sigma_e} = \frac{\alpha_n}{E\sigma_e} \tag{21}$$

in which α_n is chosen to correspond with the current value of the effective stress [27].

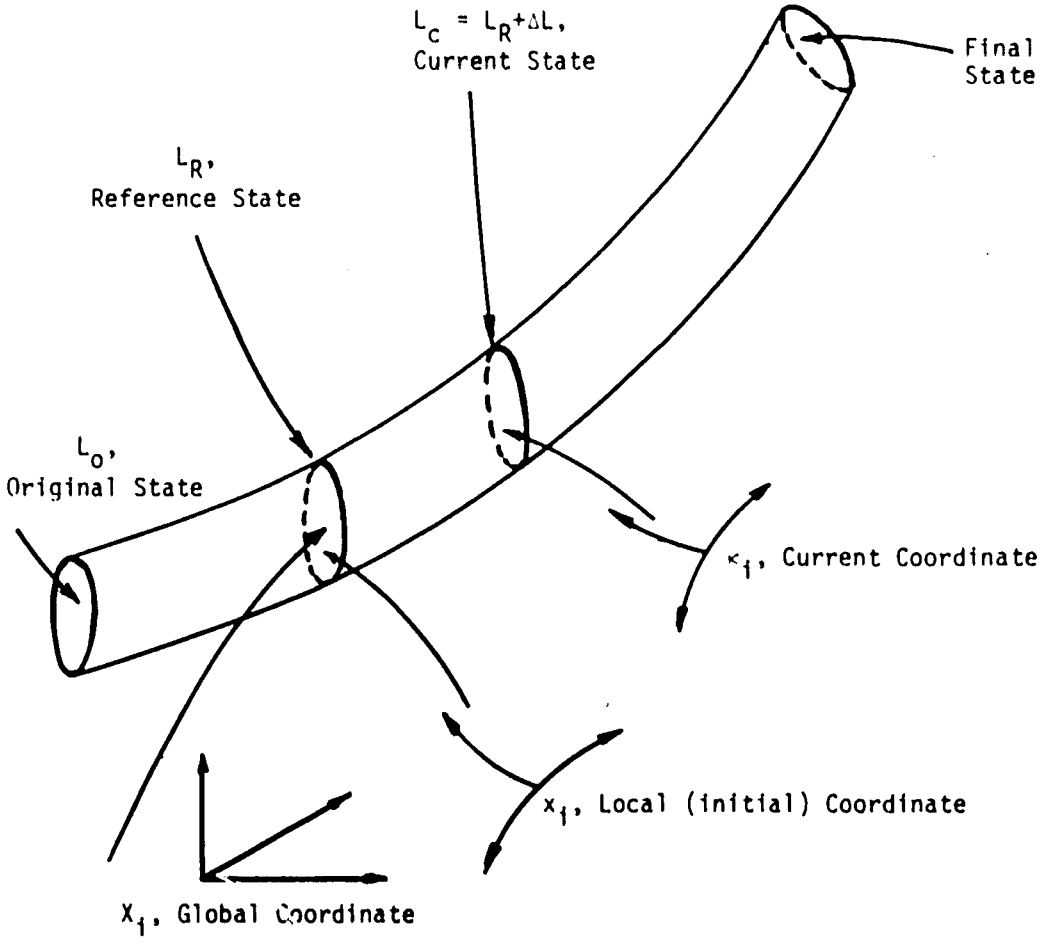

FIGURE 4 · INCREMENTAL PROCEDURE

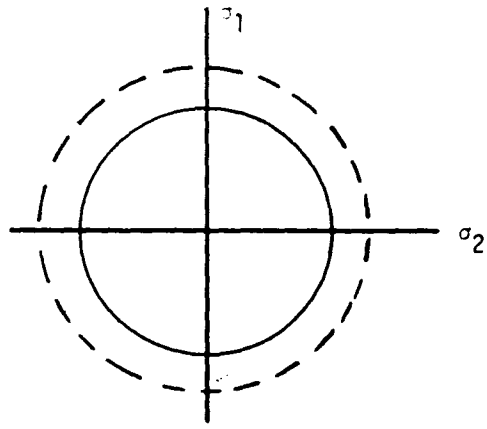

(a) Isotropic Hardening

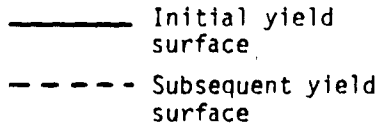

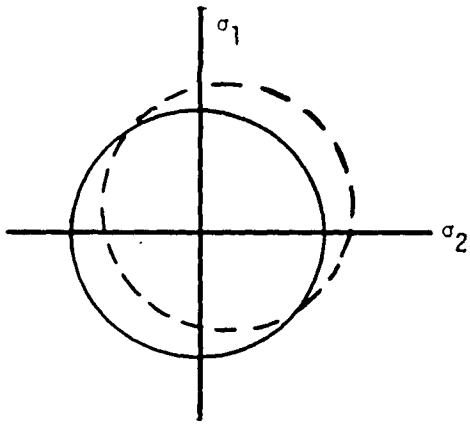

(b) Kinematic Hardening

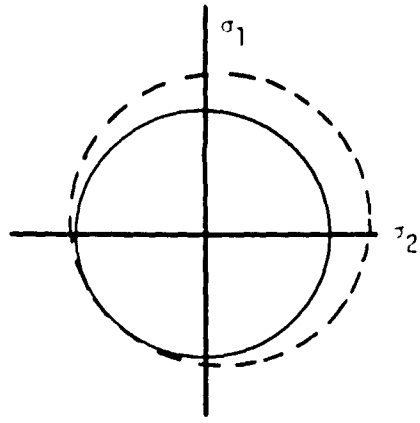

(c) Combined Hardening

FIGURE 5 - STRAIN HARDENING THEORIES

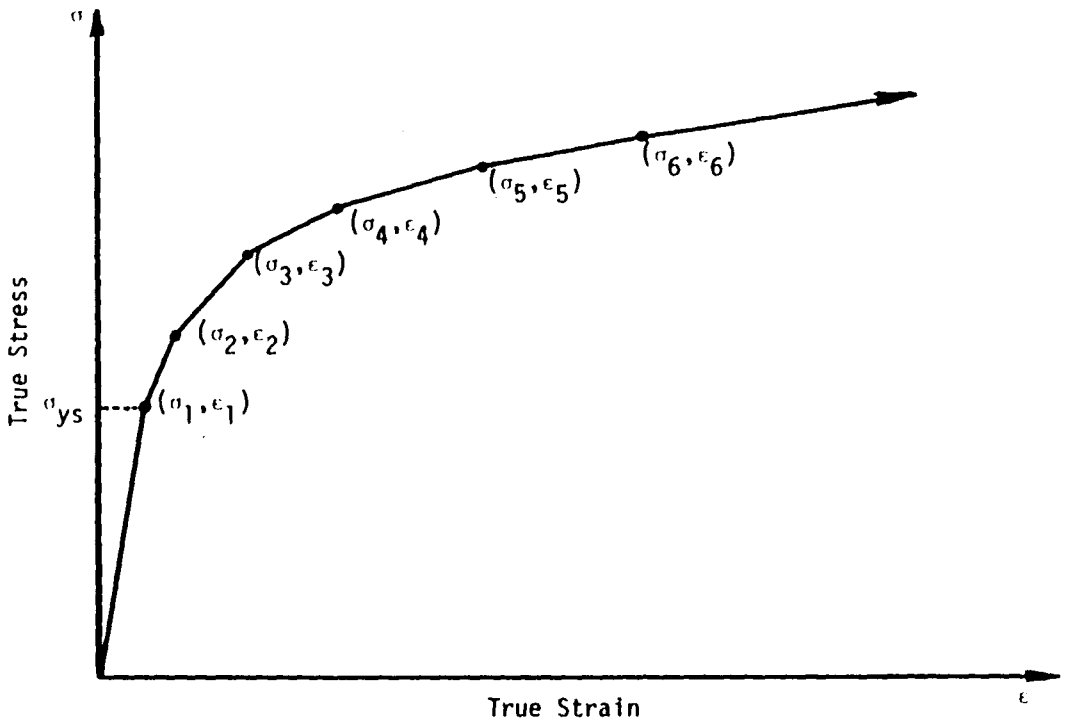

FIGURE 6 - MULTILINEAR APPROXIMATION FOR AN UNIAXIAL STRESS-STRAIN CURVE WITH STRAIN HARDENING

CHAPTER V - ITERATIVE SOLUTION PROCEDURE BY FINITE ELEMENT

The governing equations of incremental plasticity are solved by the finite element method. The system of equations is *discretized* to form a system of nonlinear algebraic equations:

$$\underset{\sim}{K}(\underset{\sim}{u}) \cdot \dot{\underset{\sim}{u}} - \dot{\underset{\sim}{R}} = 0 \tag{22}$$

where $\dot{\underset{\sim}{R}}$ is the nodal loading vector and $\dot{\underset{\sim}{u}}$ the corresponding nodal velocity vector. The stiffness matrix is

$$\underset{\sim}{K}(\underset{\sim}{u}) = \sum_{\text{elements}} \int_{\text{element area}} \underset{\sim}{B}^T \underset{\sim}{D}(\underset{\sim}{u}) \underset{\sim}{B} dA \tag{23}$$

It depends on the current nodal displacement vector through the matrix $\underset{\sim}{D}(\underset{\sim}{u})$ relating the stress and strain rates and through the matrix $\underset{\sim}{B}$ relating the strain rate to the nodal displacement rates. This nonlinear system of equations is then solved for the nodal displacements, $\underset{\sim}{u}$, for each load increment by the Newton-Raphson technique (tangent stiffness method). Convergence criteria are based on the following three factors:

(1) The mean square of the residual force vector accounts for changes in incremental stiffness due to geometric distortion and material nonlinearity. The condition

$$|F|^2 = \underset{\sim}{F} \cdot \underset{\sim}{F} \tag{24}$$

enforces global equilibrium.

(2) The mean squares of the increment load vector is

$$|\Delta R|^2 = \underset{\sim}{\Delta R} \cdot \underset{\sim}{\Delta R} \tag{25}$$

(3) The total load vector for the particular increment is

$$|R|^2 = \underset{\sim}{R} \cdot \underset{\sim}{R} \tag{26}$$

such that

$$\frac{|F|^2}{|\Delta R|^2} \leq C_1 = .05 \text{ (increment equilibrium)} \tag{27}$$

and

$$\frac{|F|^2}{|R|^2} \leq C_2 = 10^{-7} \text{ (overall equilibrium)} \tag{28}$$

Refer to [22] for more details.

CHAPTER VI - ANALYTICAL MODELING AND MATERIAL PROPERTIES

Figure 7 shows two plates joined together by a butt joint. Two heat-affected zones HAZ_1 and HAZ_2 are formed between the weld material (WM) and based material (BM). In general, the problem is three-dimensional in character. Depending on the nature of loading, certain simplifications will be introduced. For example, if the welded plate structure is sufficiently wide and undergoes cylindrical bending, then it suffices to utilize a two-dimensional analysis considering only the stress and strain variations in the thickness and longitudinal direction, while the variations in the transverse direction are assumed to be negligible.

While the mechanical properties of the BM and WM can be determined before welding by standard testing procedures, those of the HAZ and WM after welding cannot be easily evaluated. Data on mechanical properties from tests of presumably homogeneous specimens removed from welds are available. Soete and Denys [28] performed tests on small slices cut parallel to the weld. The slices are small enough that homogeneity of the metallurgical microstructure along the transverse and longitudinal direction can be assumed to be uniform. The results of these tensile tests yield useful information on the change of mechanical properties at different locations of the weld. The residual stresses are released by cutting. The following properties are found in [28]:

(1) The yield strength of the BM after welding has the lowest values in comparison with those of the HAZ and WM.

(2) The highest yield strength obtained is for the HAZ while that of the WM fell in between those for the BM and HAZ.

The mechanical properties for the BM, WM, HAZ_1 and HAZ_2 to be used in this work are given in Table 1, in which ε_f is the final strain at failure.

TABLE 1 - MECHANICAL PROPERTIES OF ZONES OF THE WELDED JOINTS

	σ_{ys} (MPa)	ε_f	$(dW/dV)_c^*$ (MJ/m^3)
BM	4.483×10^2	.117	1.891×10^2
WM	4.828×10^2	.117	1.419×10^2
HAZ_1	6.552×10^2	.0935	3.470×10^1
HAZ_2	5.517×10^2	.105	7.426×10^1

Since the chemical compositions are not altered significantly during welding, the elastic modulus and Poisson's ratio should be unaffected [29] and the values of $E = 2.069 \times 10^5$ MPa and $\nu = .3$ will be used. The Ramberg and Osgood relation with $\alpha = .2$ and $n=5$ is used:

$$\varepsilon = \begin{cases} \dfrac{\sigma}{E} & , \ \sigma \leq \sigma_{ys} \\ \dfrac{1}{E}\left[\sigma + \alpha\left(\left(\dfrac{\sigma}{\sigma_{ys}}\right)^n - 1\right)\sigma_{ys}\right], & \sigma > \sigma_{ys} \end{cases}$$

and assumed to apply for the WM, HAZ and BM with different yield strength. Refer to Figure 8. The test data in [28], however, are based on the small specimen uniaxial tensile tests by removing the WM, HAZ and BM from the weldments. They may not represent the actual situation since it is well-known that the translation of small specimen data to the larger size component structure is still not well understood even though the material microstructure is unaltered. Ductility and brittleness of a material depend sensitively on the volume to surface ratio of the specimen.

Weldment failures have been identified with cracks along the fusion line, in the WM, HAZ or in the BM itself [30]. Figure 9(a) shows a pipeline structure that is welded longitudinally. The internal pressure tends to load the joint by cylindrical bending. In this case, the weldment is entirely yielded. The objective in design is to assess the allowable load or internal pressure in terms of the construction of the weld joint. Several possibilities are shown in Figure 9(b) in which the perfectly aligned situation with no initial defects is taken as a reference, while the other cases of an edge notch, Figure 9(c), and undercut in one of the BM and a crack in the HAZ are investigated to show the difference in failure modes.

In order to have a realistic appraisal of the load carrying capacity of the weld joints shown in Figure 9, the analytical model

should include the combined influence of the BM, HAZ and WM. The dimensions of the three weld joints to be analyzed are shown in Figures 10 to 12.

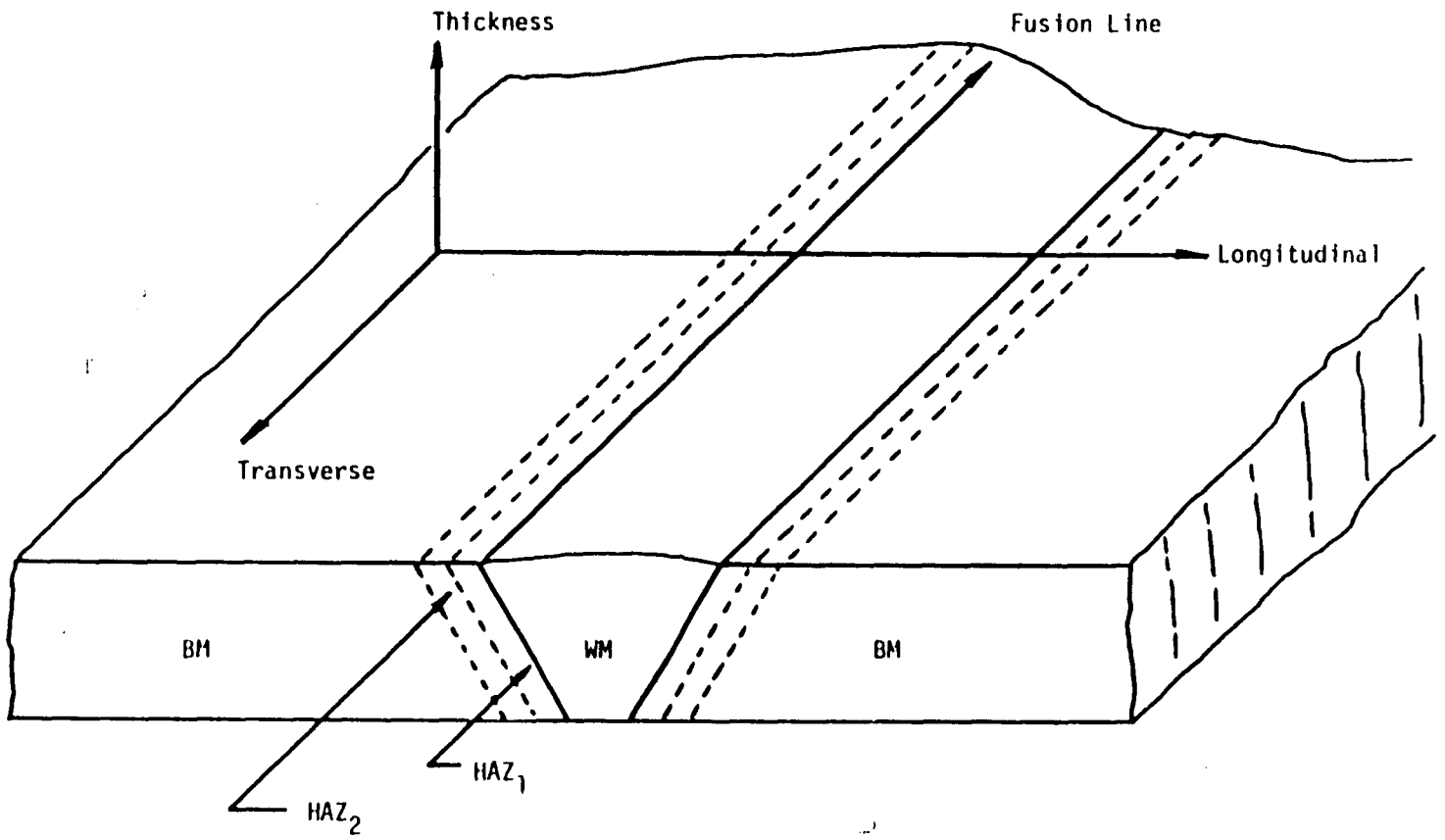

FIGURE 7 - VARIATION OF YIELD STRENGTH OF A WELD JOINT IN LONGITUDINAL DIRECTION

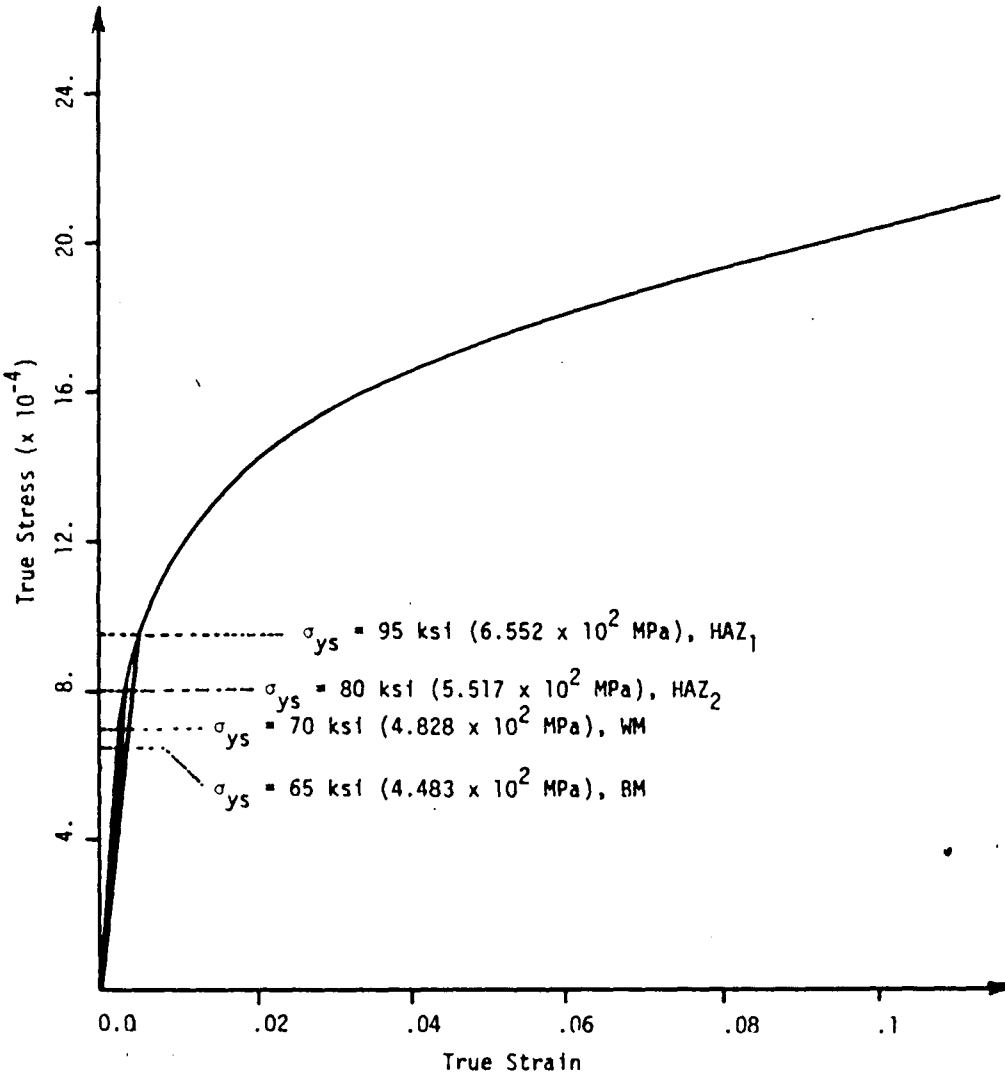

FIGURE 8 - UNIAXIAL STRESS-STRAIN CURVES FOR BM, WM, HAZ_2, HAZ_1

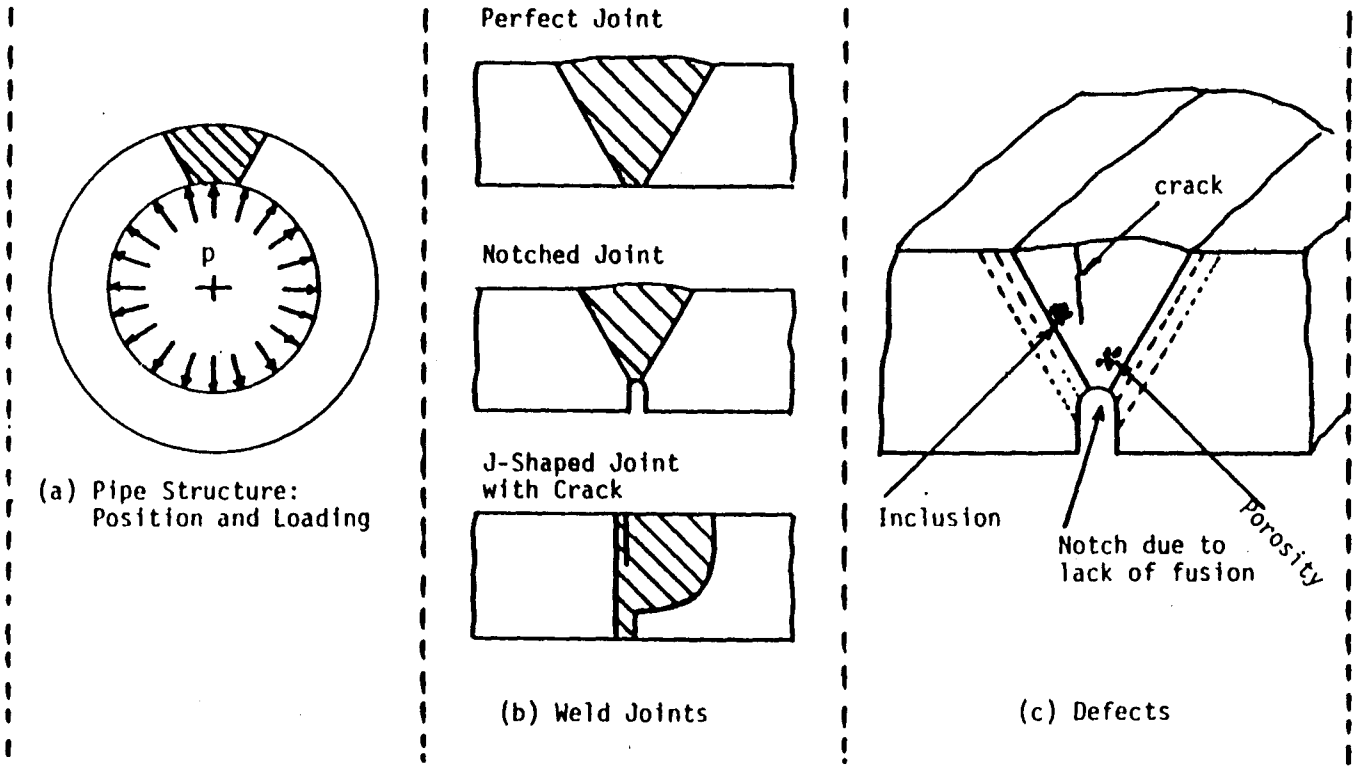

FIGURE 9 - GEOMETRIC FEATURES, LOADING AND DEFECTS IN WELDMENTS

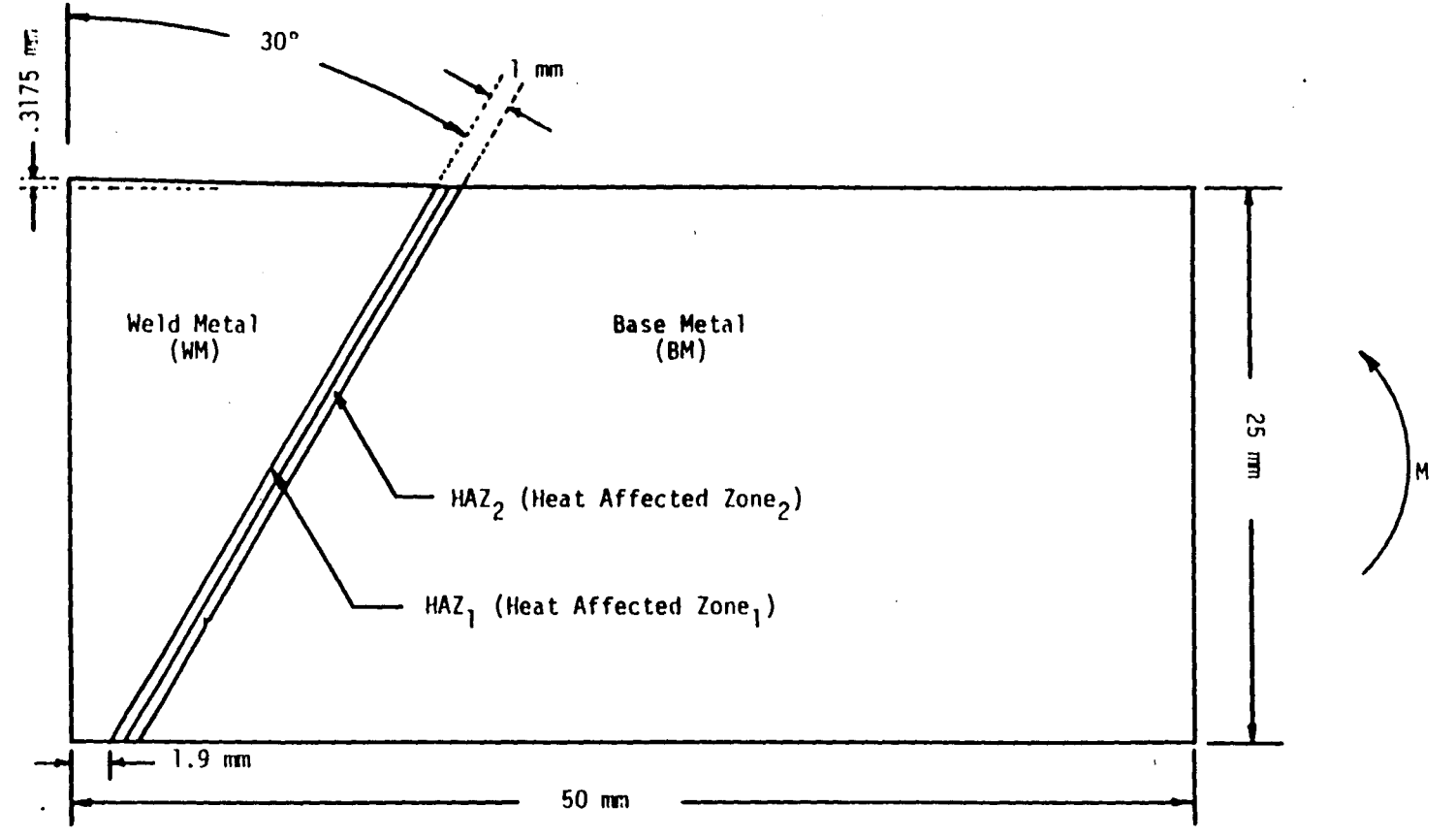

FIGURE 10 - DIMENSIONS OF THE PERFECT WELD JOINT

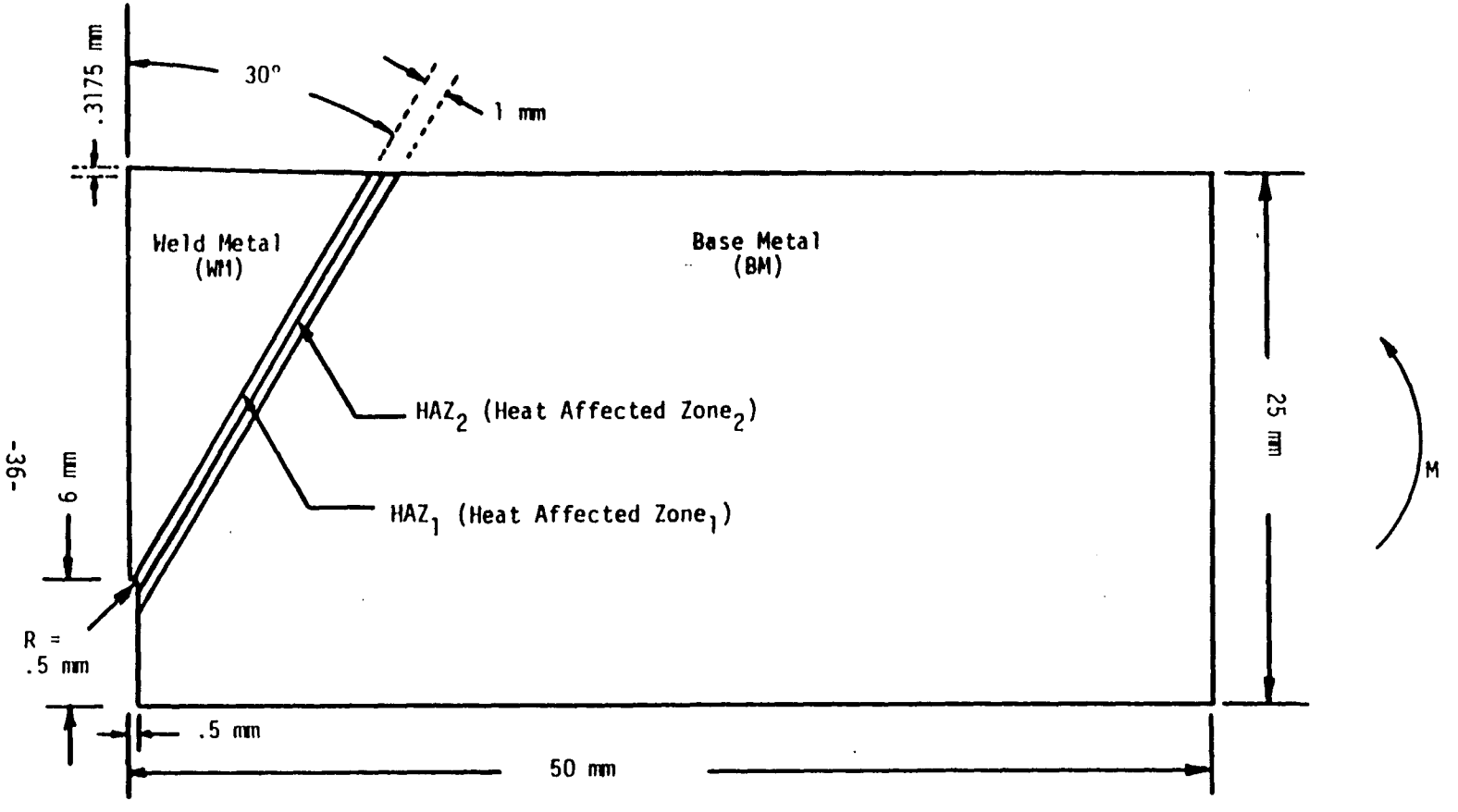

FIGURE 11 - DIMENSIONS OF THE NOTCHED WELD JOINT

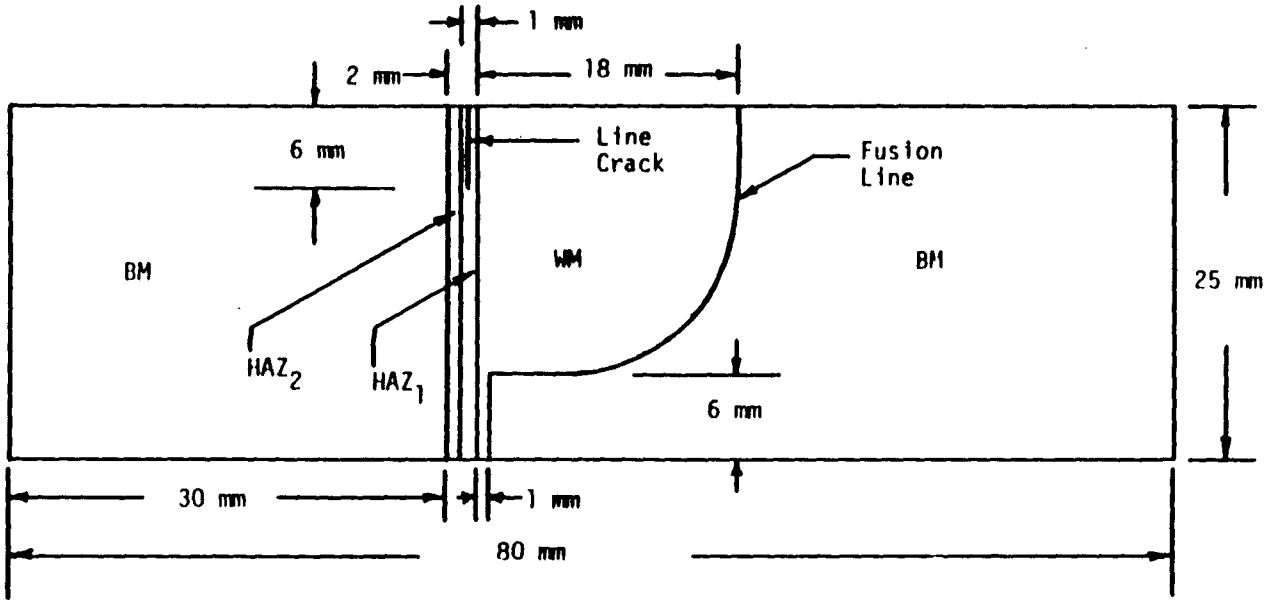

FIGURE 12 - DIMENSIONS OF THE J-SHAPED WELD JOINT WITH CRACK

CHAPTER VII - DISCUSSION OF RESULTS

The finite element grid patterns for the perfect joint, notched joint and J-shaped joint with crack are shown in Figures 13, 16 and 22, respectively. They are all subjected to pure bending loads simulated by linearly varying compressive and tensile stresses according to the simple beam formula $\sigma = M_y/I$ where M is the bending moment, y the distance from the centroidal axis and I the moment of inertia. The loading increments for the three joints are different and they are given in Table 2. The maximum applied stress for the perfect joint is $3\sigma^*$, the notched joint is $1.6\sigma^*$ and J-shaped joint with crack os $0.9\sigma^*$ where $\sigma^* = 6.897 \times 10^2$ MPa.

Perfect Joint (Figures 10 and 13). The finite element results for this weld configuration are summarized in Figures 14 and 15 in terms of the effective stress σ_{eff}* and strain energy density dW/dV contours. Figure 14 gives nine σ_{eff} contours with magnitude from 2.758×10^2 to 1.310×10^3 MPa. Referring to Table 1, the stress states corresponding to contours 5 to 9 are beyond the yield strength σ_{ys} of the WM, BM and HAZ. The intensity of yielding increases as the surfaces of the plates are approached. Contours of constant strain energy density are displayed in Figure 15. Relative minima of dW/dV or $(dW/dV)_{min}$ are sited at five (5) different

---

*The effective stress $\sigma_{eff} = \sqrt{3J_2}$ where J_2 is the flow criterion of von Mises.

TABLE 2 - RATE OF LOADING OF THE THREE WELD JOINTS

Increment Number	Perfect Joint σ^* (MPa)	Notched Joint σ^* (MPa)	J-Shaped Joint with Crack σ^* (MPa)
1	5.067×10^2	7.528×10^1	3.419×10^1
2	5.517×10^2	1.379×10^2	1.379×10^2
3	5.862×10^2	2.069×10^2	2.069×10^2
4	6.207×10^2	2.758×10^2	2.758×10^2
5	6.552×10^2	3.448×10^2	3.448×10^2
6	6.635×10^2	4.138×10^2	4.138×10^2
7	6.724×10^2	4.827×10^2	4.827×10^2
8	6.793×10^2	5.517×10^2	5.517×10^2
9	6.897×10^2	6.207×10^2	6.207×10^2
10	7.586×10^2	6.897×10^2	
11	8.276×10^2	7.586×10^2	
12	8.966×10^2	8.276×10^2	
13	9.656×10^2	8.966×10^2	
14	1.034×10^3	9.656×10^2	
15	1.103×10^3	1.034×10^3	
16	1.206×10^3	1.103×10^3	
17	1.379×10^3		
18	1.551×10^3		
19	1.724×10^3		
20	1.896×10^3		
21	1.965×10^3		
22	2.069×10^3		

locations. Those labelled 1 and 2 are maximum values of the local* minima $(dW/dV)_{min}^{max}$ in the WM and HAZ and those labelled 3, 4 and 5 are global minima with 3 being in the WM, 4 in HAZ and 5 in the BM. At maximum load of $3 \times \sigma^* = 6.897 \times 10^2$ MPa, the values of $(dW/dV)_{min}^{max}$ at sites 1 and 2 are 4.276 MJ/m^3 and 5.241 MJ/m^3, respectively, which are well below the threshold values of $(dW/dV)_c^*$ given in Table 1. With an increasing applied load or bending, the $(dW/dV)_{min}^{max}$ value at site 2 will first reach $(dW/dV)_c^*$ in the HAZ before site 1 becomes critical. This prediction tends to agree with the experimental observation obtained recently for high strength weldments. Fracture was seen to initiate and propagate along the weld seams or HAZ [31].

The locations of the global $(dW/dV)_{min}$ appear near the central axis of the welded structure. The interaction between the local and global $(dW/dV)_{min}$ determines the termination of local failure and the beginning of global instability at which point the welded structure collapses entirely. The precise relationship is beyond the scope of this study.

Notched Joint (Figures 11 and 16). Figure 17 gives an overall view of the σ_{eff} contours when the weld joint contains a notch on

*The local minimum of dW/dV should be distinguished from the global minimum. The former refers to a system of coordinates within the system, and the latter a system of coordinates viewed from outside.

the tension side of the bent structure. Yielding becomes more pronounced as the notch tip is approached. The region corresponding to contours 7, 8, 9, etc., is well within yield. An enlarged view of the notch tip region is given in Figure 18 in which the local σ_{eff} is shown to be 1.793×10^3 MPa which is several times larger than the yield strength of the WM.

Of interest is the strain energy density contours near the notch which can yield information on fracture initiation. There are four (4) $(dW/dV)_{min}$ locations, as indicated in Figure 16. Sites 1 and 2 are the local $(dW/dV)_{min}^{max}$ occurring in the WM and HAZ_1, respectively. In the WM, $(dW/dV)_{min}^{max} = 1.517 \times 10^2$ MJ/m^3 which is substantially higher than the value of 4.276 MJ/m^3 when the notch was absent, Figure 13.

This has exceeded the critical $(dW/dV)_c^* = 1.419 \times 10^2$ MJ/m^3 for the WM in Table 1. Similarly, $(dW/dV)_{min}^{max} = 6.621 \times 10^1$ MJ/m^3 in the HAZ_1, also exceeded its corresponding threshold of $(dW/dV)_c^* = 3.470 \times 10^1$ MJ/m^3, whereas without the notch, the local $(dW/dV)_{min}^{max}$ is only 5.241 MJ/m^3, Figure 13. The influence of the notch is seen to be very significant. These values correspond to a maximum stress of $1.6 \times (\sigma^* = 6.897 \times 10^2$ MPa). Figures 20 and 21 illustrate that dW/dV is a function of the radius distance r from the notch tip shown in Figure 19. At r = .3 mm, $(dW/dV)_{min}^{max}$ $= 1.517 \times 10^2$ MJ/m^3 occurred at $\theta = 0°$, (Figure 20), while at r = .56 mm $(dW/dV)_{min}^{max} = 6.621 \times 10^1$ MJ/m^3 corresponding to $\theta = 105°$. The energy density increases with decreasing r. This result is to

be expected.

The global minima of dW/dV occur at distances much further away from the notch tip and hence their values are correspondingly lower. In Figures 16 and 19, they are labelled as regions 3 and 4 with $(dW/dV)_{min}$ = .475900 MJ/m^2 and .001034 MJ/m^3, respectively.

J-Shaped Joint with Crack (Figures 12 and 22). Consider the joint configuration in Figure 12 in which one of the BM is undercut while an edge crack prevails in the HAZ_1 next to HAZ_2. Referring to Figures 12 and 22, the joint is subjected to bending stresses such that the edge crack appears in the tension side with a maximum stress value of 0.9 x (σ^* = 6.897 x 10^2 MPa). The σ_{eff} contours in Figure 23 show that yielding is now confined locally to the material near the crack tip. The values of σ_{eff} in the dark region are in the range of 7.586 x 10^2 to 1.793 x 10^3 MPa, well above the yield strength of the HAZ_1, Table 1. The enlarged view of the HAZ_1 with an edge crack is shown in Figure 24. Note that the entire HAZ_1 is yielded with increasing intensity of σ_{eff} as the crack tip is approached. At contour No. 12, the effective stress is more than twice the yield stress of the HAZ_1 material.

The strain energy density contours near the crack tip are displayed in Figure 25. The values of dW/dV are clearly seen to increase with decreasing r, the distance measured from the crack tip. For r = 0.075 mm, three local minima of dW/dV are found, as illustrated in Figure 26. They are $(dW/dV)_{min}$ = 4.000 x 10^1 MJ/m^3 at

$\theta = 0°$, 4.621×10^{1} MJ/m^3 at $\theta = -122°$ and 4.965×10^{1} MJ/m^3 at $\theta = 124°$. The maximum value of the local $(dW/dV)_{min}$ will be denoted as $(dW/dV)_{min}^{max} = 4.965 \times 10^{1}$ MJ/m^3. Although all three of these values surpassed the critical $(dW/dV)_c = 3.470 \times 10^{1}$ MJ/m^3 for the HAZ_1, fracture initiation would have first occurred in the direction of $\theta = 124°$ corresponding to the location of $(dW/dV)_{min}^{max}$ while the load is increased up to the maximum value of $0.9 \times (\sigma^* = 6.897 \times 10^{2}$ MPa).

This example shows that fracture initiation favors the side where the BM was undercut. Such information is useful for optimizing the geometric, loading and material parameters.

Local Minima

Region 1 - 4.276 (MJ/m^3)

Region 2 - 5.241

Global Minima

Region 3 - 1.517×10^{-4}

Region 4 - 3.172×10^{-4}

Region 5 - 1.862×10^{-4}

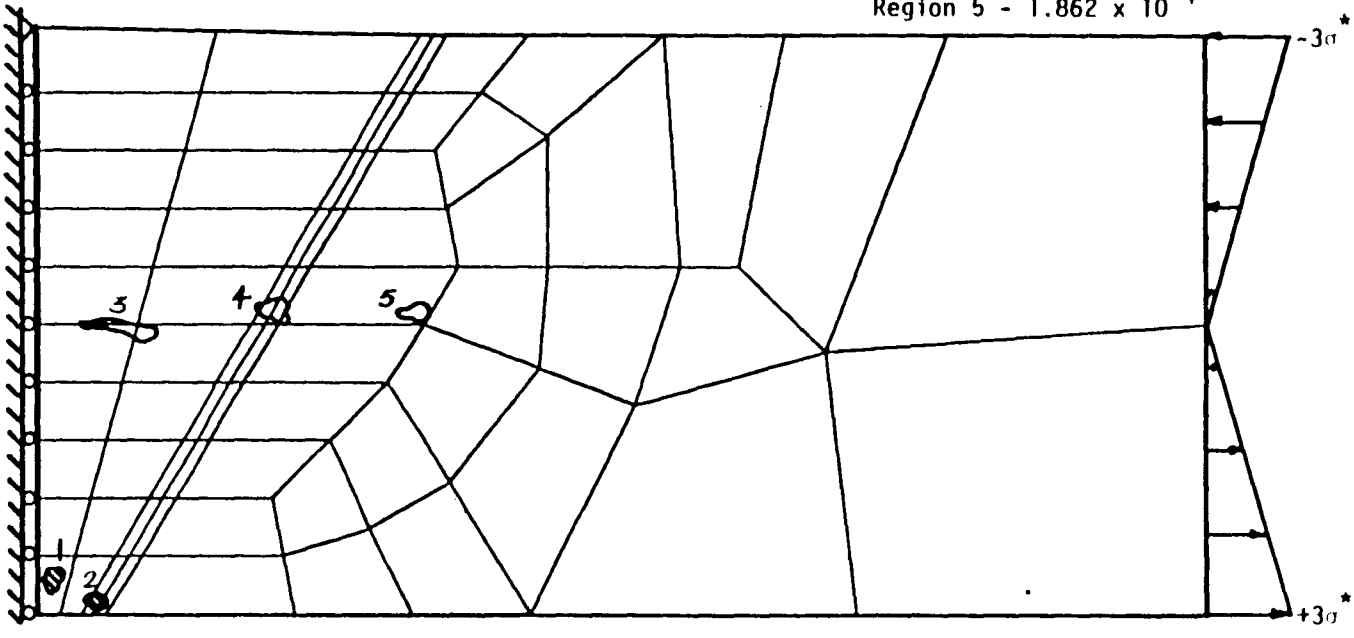

FIGURE 13 - FINITE ELEMENT GRID PATTERN AND LOCATIONS OF LOCAL AND GLOBAL $(dW/dV)_{min}$

Contour No. 1 - 2.758×10^2 MPa

Contour No. 2 - 3.655×10^2 MPa

Contour No. 3 - 4.483×10^2 MPa

Contour No. 4 - 5.379×10^2 MPa

Contour No. 5 - 6.897×10^2 MPa

Contour No. 6 - 9.656×10^2 MPa

Contour No. 7 - 1.103×10^3 MPa

Contour No. 8 - 1.241×10^3 MPa

Contour No. 9 - 1.310×10^3 MPa

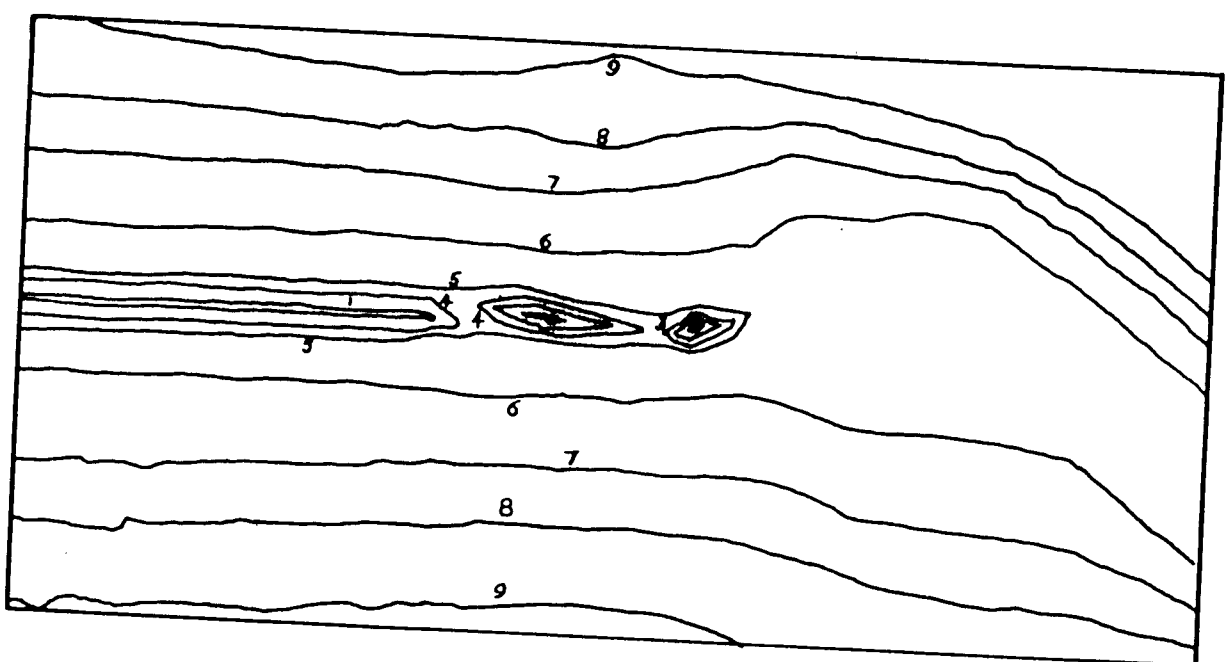

FIGURE 14 - EFFECTIVE STRESS CONTOURS AT $3\sigma^*$

Contour No. 1 - 4.276 (MJ/m^3)

Contour No. 2 - 5.241 (MJ/m^3)

Contour No. 3 - 1.517×10^{-4}

Contour No. 4 - 3.172×10^{-4}

Contour No. 5 - 1.862×10^{-4}

Contour No. 6 - 2.345×10^{-1}

Contour No. 7 - 5.517×10^{-1}

Contour No. 8 - 1.103

Contour No. 9 - 2.207

Contour No. 10 -

Contour No. 11 -

Contour No. 12 -

Contour No. 13 -

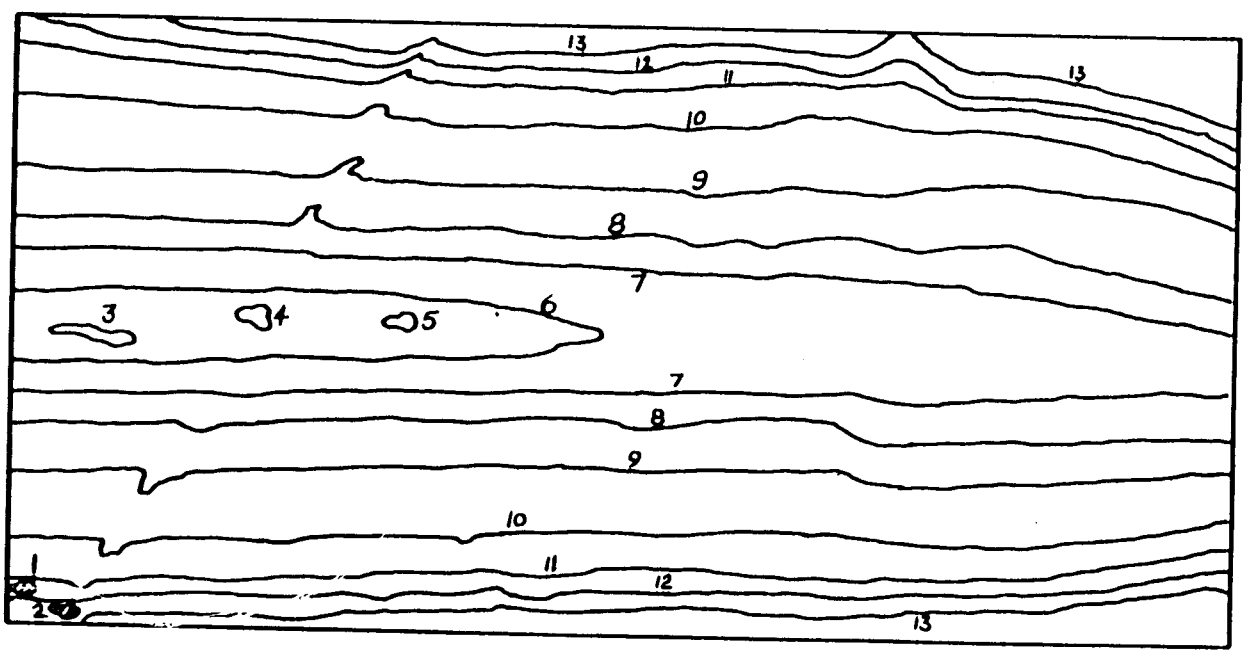

FIGURE 15 - STRAIN ENERGY DENSITY CONTOURS AT $3\sigma^*$

Local Minima

Region 1 - 1.517×10^2 (MJ/m^3)

Region 2 - 6.621×10^1

Global Minima

Region 3 - .475900

Region 4 - .001034

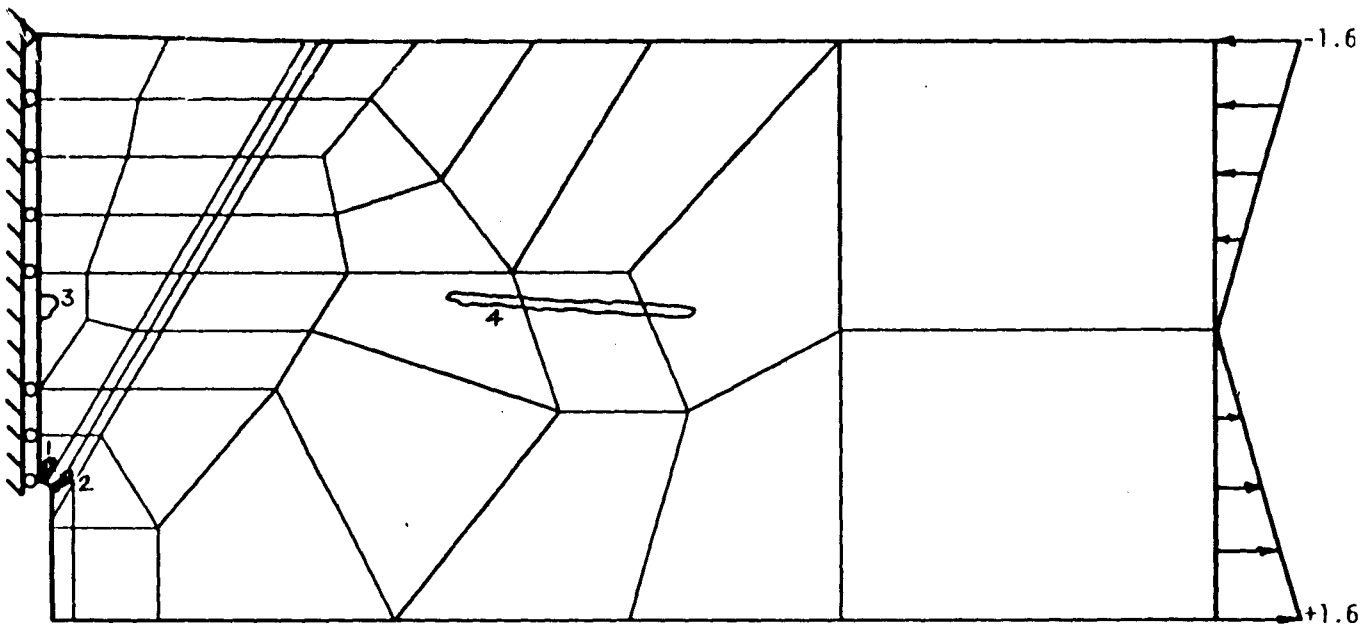

FIGURE 16 - FINITE ELEMENT GRID PATTERN AND LOCATION OF LOCAL AND GLOBAL $(dW/dV)_{min}$

Contour No. 1 - 1.172 x 10^2 (MPa)

Contour No. 2 - 2.069 x 10^2

Contour No. 3 - 2.896 x 10^2

Contour No. 4 - 3.793 x 10^2

Contour No. 5 - 4.690 x 10^2

Contour No. 6 - 5.517 x 10^2

Contour No. 7 - 6.414 x 10^2

Contour No. 8 - 7.586 x 10^2

Contour No. 9 - 8.276 x 10^2

Contour No. 10- 8.966 x 10^2

Contour No. 11- 9.655 x 10^2

Contour No. 12- 1.103 x 10^3

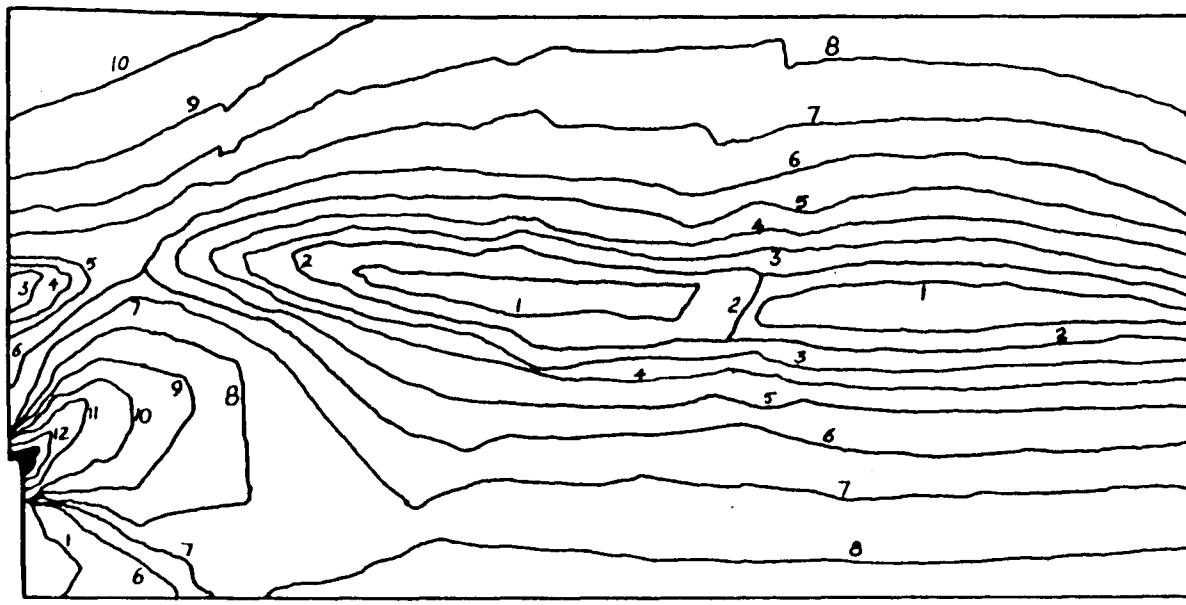

FIGURE 17 - EFFECTIVE STRESS CONTOURS AT $1.6\sigma^*$

Contour No. 1 - 6.414 x 10^2 (MPa)
Contour No. 2 - 6.897 x 10^2
Contour No. 3 - 8.276 x 10^2
Contour No. 4 - 8.966 x 10^2
Contour No. 5 - 9.656 x 10^2
Contour No. 6 - 1.034 x 10^3
Contour No. 7 - 1.103 x 10^3
Contour No. 8 - 1.241 x 10^3
Contour No. 9 - 1.310 x 10^3
Contour No. 10- 1.379 x 10^3
Contour No. 11 - 1.448 x 10^3
Contour No. 12 - 1.517 x 10^3
Contour No. 13 - 1.586 x 10^3
Contour No. 14 - 1.724 x 10^3
Contour No. 15 - 1.793 x 10^3

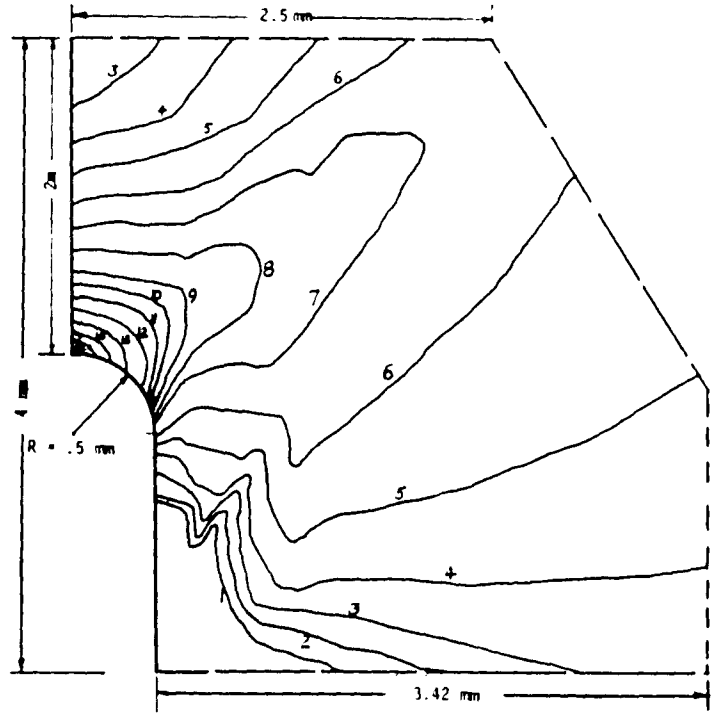

FIGURE 18 - EFFECTIVE STRESS CONTOURS AROUND THE NOTCH AT 1.6σ

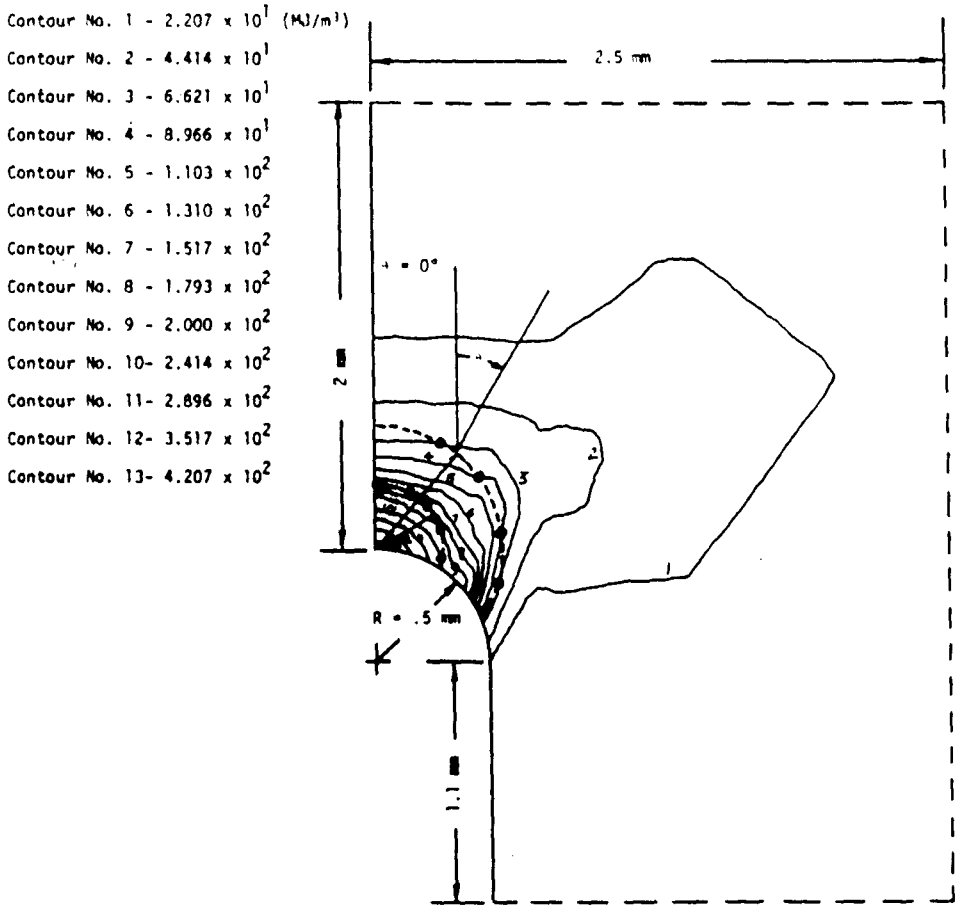

FIGURE 19 - RADIUS VECTOR LOCI INTERSECTING STRAIN ENERGY DENSITY CONTOURS FOR $r = .3$ AND $r = .56$ mm

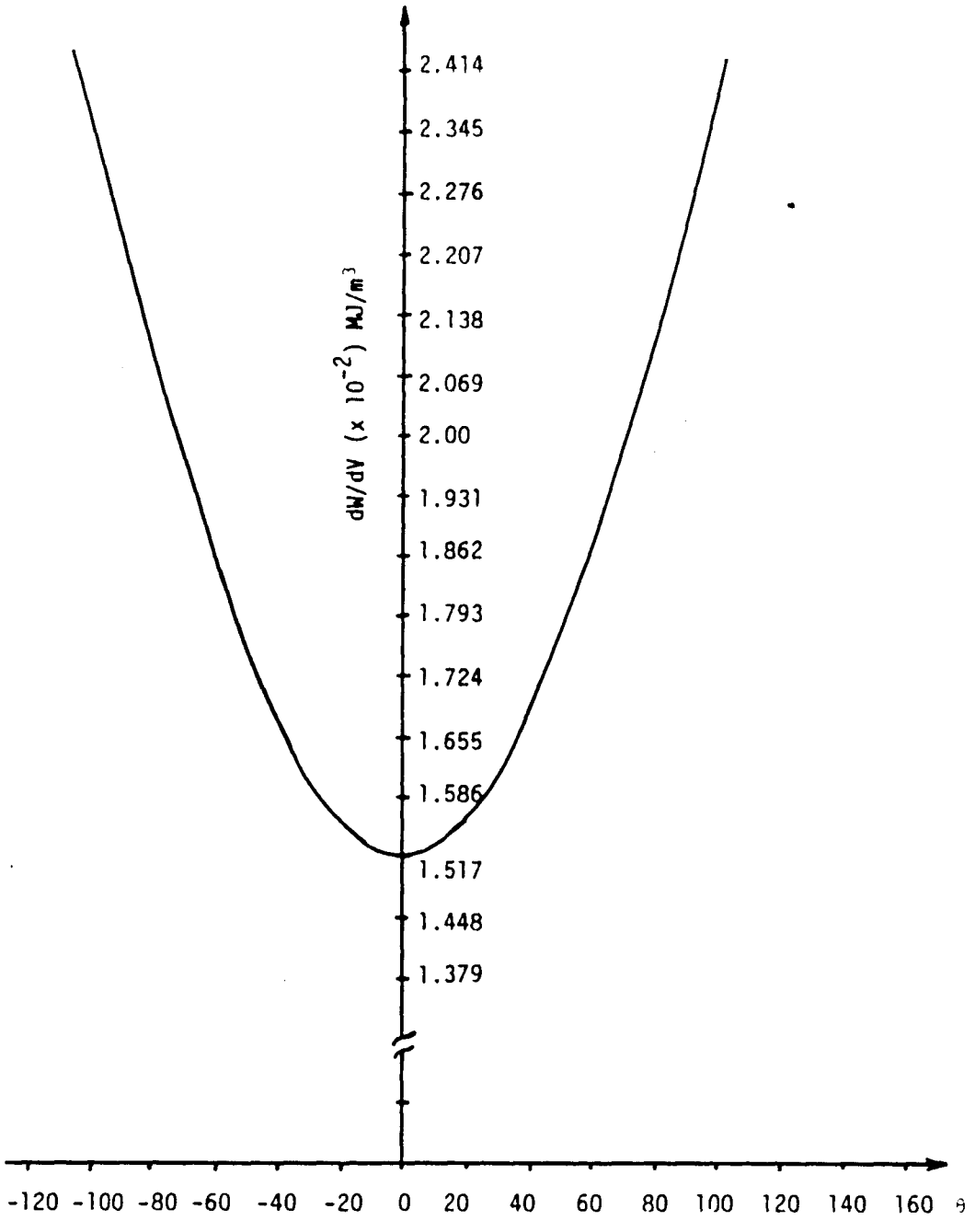

FIGURE 20 - VARIATION OF dW/dV FOR CONSTANT MAGNITUDE RADIUS VECTOR, (r = .3 mm) AS FUNCTION OF POLAR ANGLE

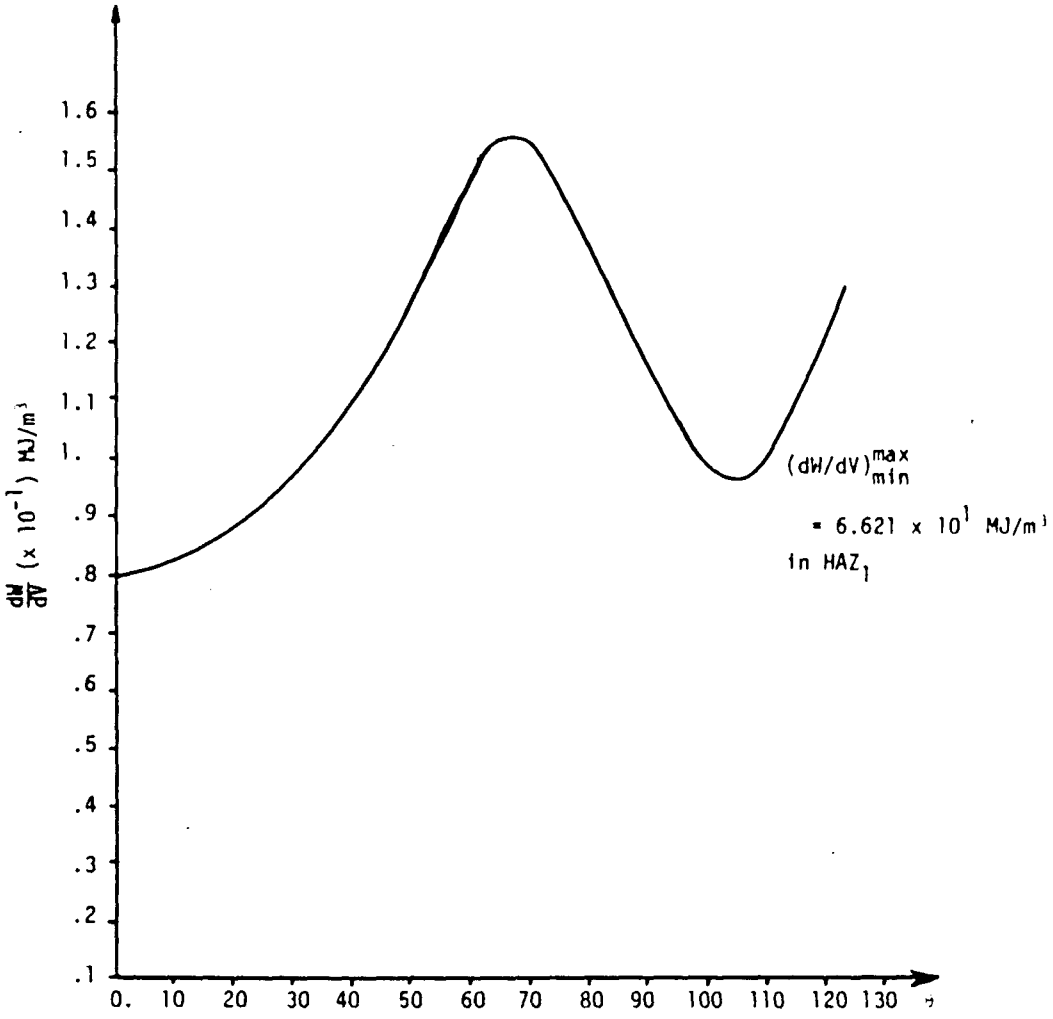

FIGURE 21 - VARIATION OF dW/dV FOR CONSTANT MAGNITUDE RADIUS VECTOR, (r = .56 mm) AS FUNCTION OF POLAR ANGLE

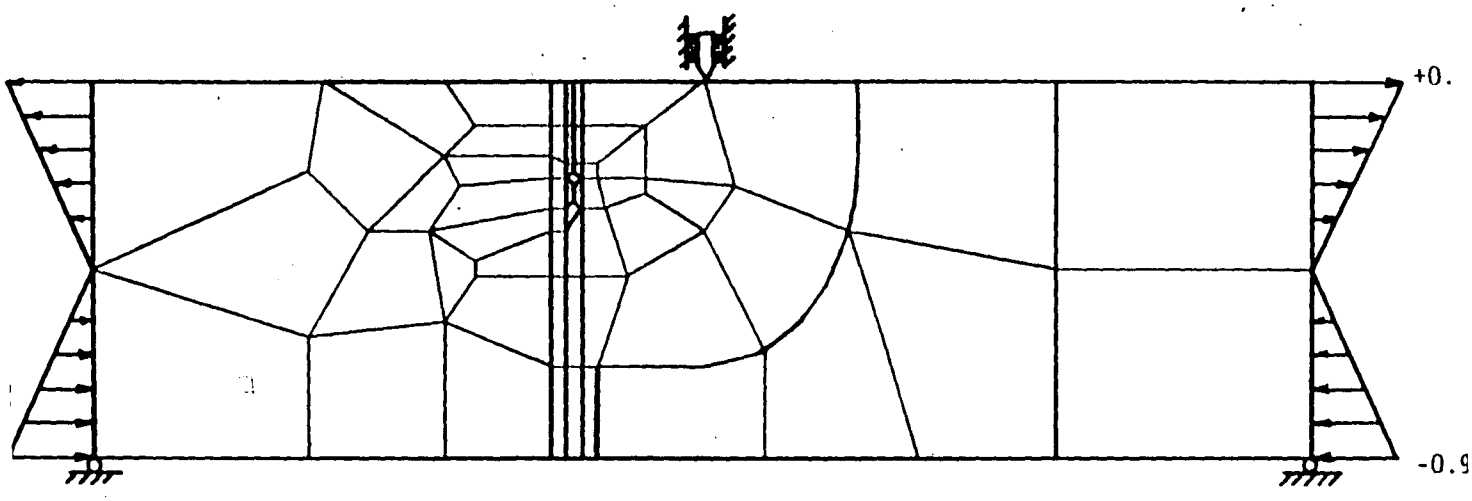

FIGURE 22 - FINITE ELEMENT GRID PATTERN OF THE J-SHAPED WELD JOINT WITH A CRACK

Contour No. 1 - 8.966×10^{1} (MPa)

Contour No. 2 - 1.724×10^{2}

Contour No. 3 - 2.483×10^{2}

Contour No. 4 - 3.310×10^{2}

Contour No. 5 - 4.138×10^{2}

Contour No. 6 - 4.966×10^{2}

Contour No. 7 - 5.724×10^{2}

Contour No. 8 - 6.552×10^{2}

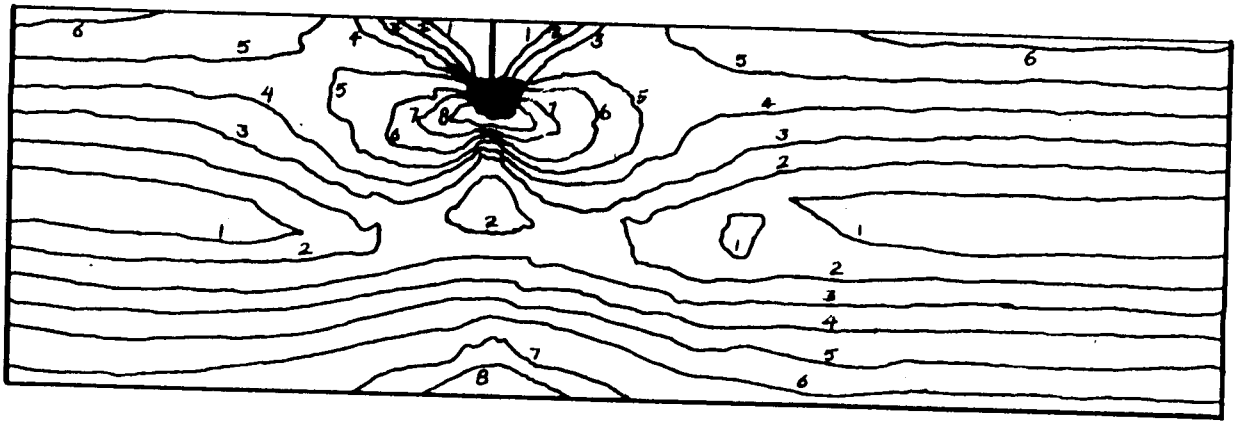

FIGURE 23 - EFFECTIVE STRESS CONTOURS AT $.9\sigma^{*}$

Contour No.

1. 5.655×10^2 (MPa)
2. 6.345×10^2
3. 6.897×10^2
4. 7.586×10^2
5. 8.276×10^2
6. 8.966×10^2
7. 9.656×10^2
8. 1.034×10^3
9. 1.103×10^3
10. 1.172×10^3
11. 1.241×10^3
12. 1.517×10^3

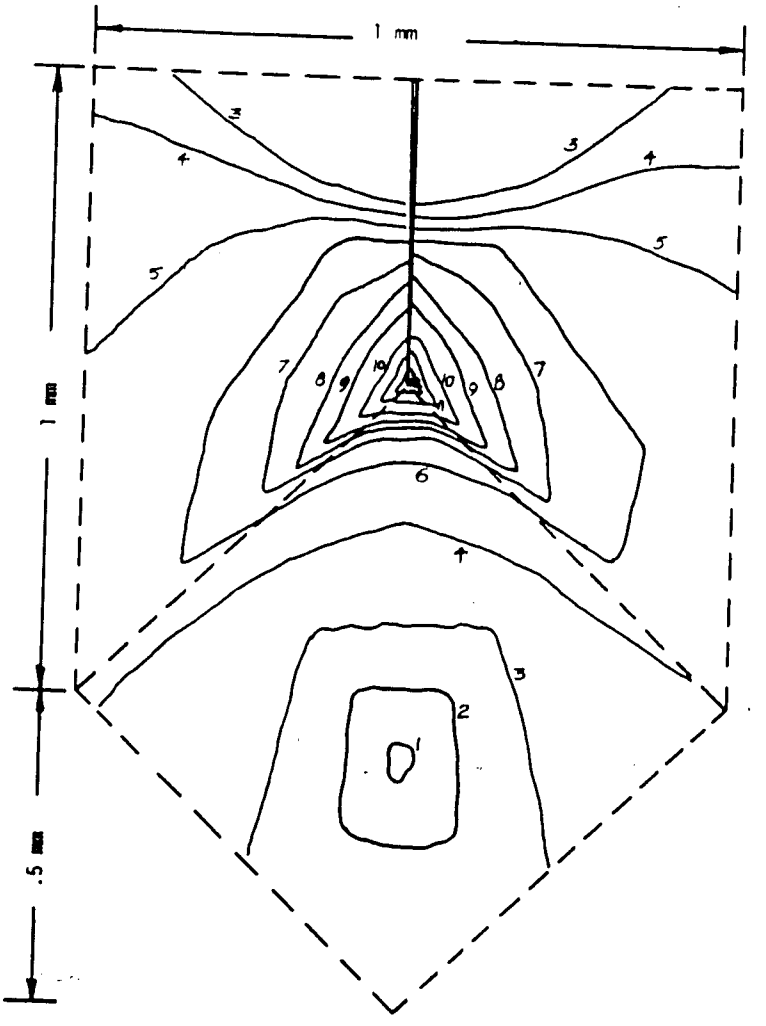

FIGURE 24 - EFFECTIVE STRESS CONTOURS AT $.9\sigma^*$ AROUND THE CRACK TIP

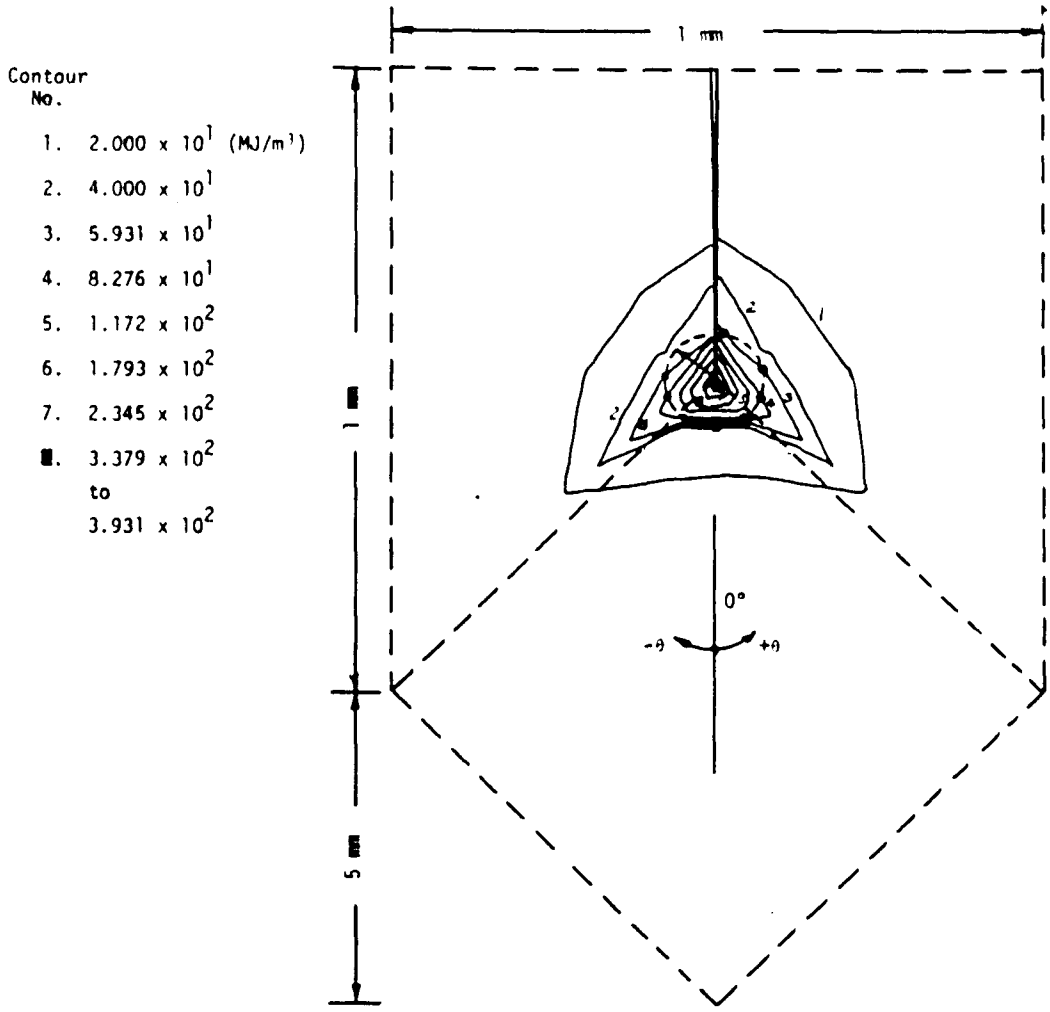

FIGURE 25 - RADIUS VECTOR LOCUS INTERSECTING STRAIN ENERGY DENSITY CONTOURS (r = .075 mm)

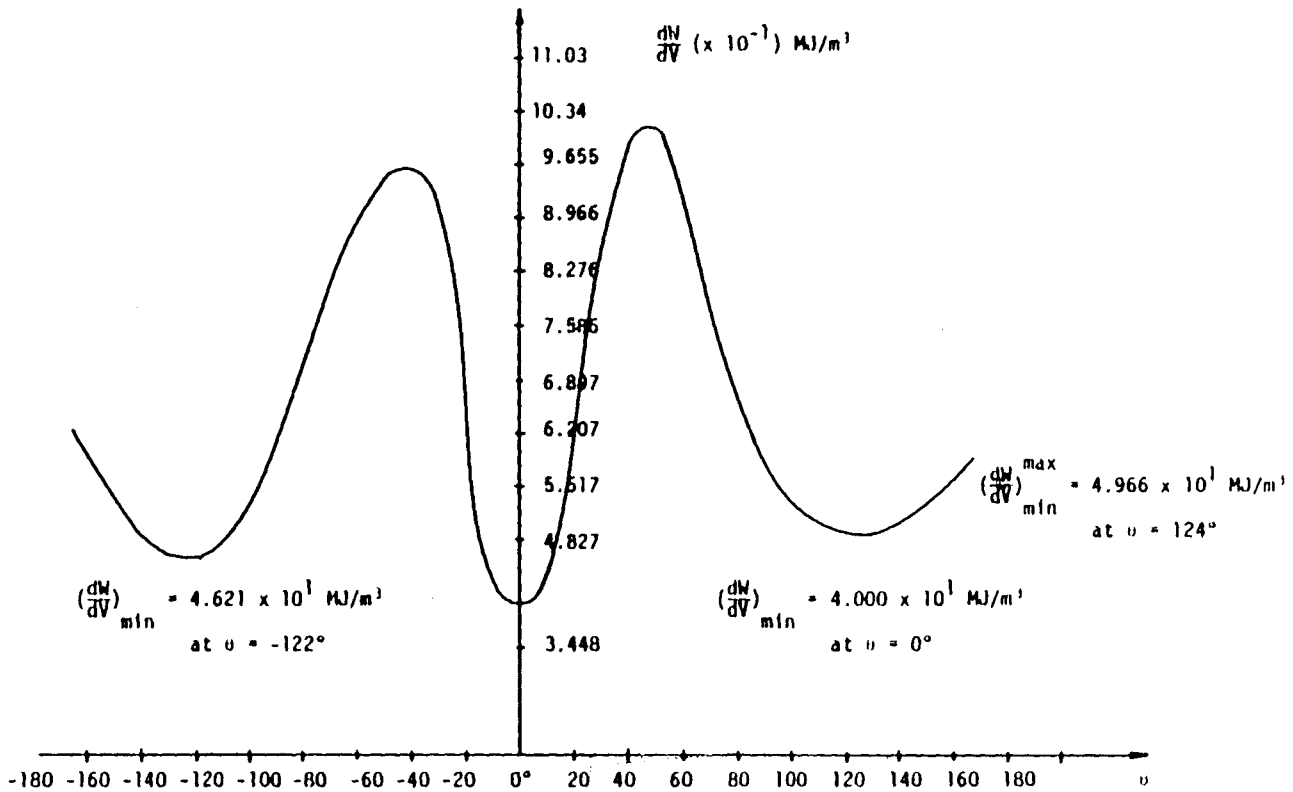

FIGURE 26 - VARIATION OF (dW/dV) FOR CONSTANT MAGNITUDE VECTOR, r = .075 mm (ALL IN HAZ_1) FUNCTION OF POLAR ANGLE

CHAPTER VIII - CONCLUSIONS

The prediction of possible failure sites in welded joints has been carried out in this study by application of the strain energy density theory and the incremental theory of plasticity. Because most weld joints undergo gross yielding during service, their local transfer characteristics are inherently dependent on the load history. The standard specimen testing procedure is not adequate because, in principle, weldment integrity can only be determined under actual loading conditions.

Three different joint configurations are investigated with increasing severity in terms of the type of mechanical defects encountered in weldment fabrication. The perfect joint is analyzed for reference purpose. The decreasing load-carrying capacity of the welded structure is determined for a joint with a notch and a crack in the HAZ. The strain energy density criterion is applied consistently to all three joint configurations such that the loading, geometric and material parameters can be studied in a combined fashion. The analytical procedure can be used to optimize weldment design. Once the failure initiation sites are found, damage growth by yielding and crack growth up to global instability of the weldment can also be carried out by the strain energy density theory.

Lacking at present are realistic data of $(dW/dV)_c$ and $(dW/dV)_c^*$ values of the WM, HAZ and BM. Experiments, however, will have to

be designed in accordance with additional analytical results on weld joints loaded up to final separation. The effect of loading rates will have to be first studied analytically.

REFERENCES

[1] Masubuchi, K., Analysis of Welded Structures, Pergamon Press, Ltd., 1980.

[2] Thielsch, H., "When are Weld Defects Rejectable?", Materials Evaluation, February and March, 1969.

[3] Vinovkurov, A. V., "The Use of Fracture Mechanics Assumptions for Evaluating the Properties of Welded Joints", Svar. Proiz., No. 5, pp. 2-4, 1977.

[4] Dawes, M. G., "Fracture Control in High Yield Strength Weldments", Welding Journal, 53 (9), 369s-379s, 1974.

[5] Sih, G. C., "Some Basic Problems in Fracture Mechanics and New Concepts", Engineering Fracture Mechanics, 5, pp. 365-377, 1973.

[6] Sih, G. C., "A Special Theory of Crack Propagation: Methods of Analysis and Solution of Crack Problems", Mechanics of Fracture I, edited by G. C. Sih, Noordhoff International Publishing, Leyden, pp. XXI-XLV, 1973.

[7] Sih, G. C., "Mechanics of Ductile Fracture", IFSM-77-78, Lehigh University, 1977.

[8] Turner, C. E., in Post Yield Fracture, ed. D. G. H. Latzgo, Appl. Sci. Pub. Ltd., p. 23, 1979.

[9] Dugdale, D. S., J. Mech. Phys. Sol., Vol. 8, p. 100, 1960.

[10] Kamath, M. S., Woodley, C. C. and Harrison, J. D., "The Application of Fracture Mechanics to Welded Structures", Fracture Mechanics in Engineering Application, edited by G. C. Sih, S. R. Valluri, Sijthoff and Noordhoff, The Netherlands, pp. 809-830, 1979.

[11] Wells, A. A., "The Application of Fracture Mechanics at and beyond General Yielding", British Welding Journal, p. 563, 1963.

[12] Radon, J. C. and Czoboly, E., "Material Toughness Versus Specific Fracture Work", Int. Conf. on Mechanical Behavior of Materials, Vol. I, p. 543, 1971.

[13] Dawes, M. G., "Elastic-Plastic Fracture Toughness Based on the COD and J-Contour Integral Concepts", Elastic-Plastic Fracture, ASTM STP 668, J. D. Landes, J. A. Begley and G. A. Clarke, eds., American Society for Testing and Materials, pp. 307-333, 1979.

[14] Harrison, J. D., Dawes, M. G., Archer, G. L. and Kamath, M. S., "The COD Approach and Its Application to Welded Structures", Elastic-Plastic Fracture, ASTM STP 668, J. D. Landes, J. A. Begley and G. A. Clarke, eds., American Society for Testing and Materials, pp. 606-631, 1979.

[15] Gillemot, L. F., "Criterion of Crack Initiation and Spreading", J. of Engineering Fracture Mechanics, Vol. 8, pp. 239-253, 1976.

[16] Sih, G. C., "Energy Density Concept in Fracture Mechanics", Engineering Fracture Mechanics, 5, pp. 1037-1040, 1973.

[17] Sih, G. C., "Strain Energy Density Factor Applied to Mixed Mode Crack Problems", International Journal of Fracture, 10, pp. 300-321, 1974.

[18] Sih, G. C., "Analytical Modeling: Crack Growth Characteristics", Fracture Mechanics, edited by N. Perrone, H. Liebowitz, D. Mulville and W. Pilkey, University Press of Virginia, Charlottesville, 1978.

[19] Kipp, M. E. and Sih, G. C., "The Strain Energy Density Failure Criterion Applied to Notched Elastic Solids", Int. J. of Solids and Structures, Vol. 11, pp. 153-173, 1975.

[20] Theocaris, P. S., "Experimental Determination of the Core Region in Mixed Mode Fracture", Proceedings of the First USA-Greece Symposium on Mixed Mode Crack Propagation, edited by G. C. Sih and P. S. Theocaris, Sijthoff and Noordhoff, pp. 21-36, 1981.

[21] Pu, S. L., Hussain, A. M. and Lorensen, W. E., "The Collapsed Cubic Isoparametric Element as a Singular Element for Crack Problems", Int. J. for Numerical Met. in Engineering, Vol. 12, pp. 1721-1742, 1978.

[22] Gifford, L. N. and Hilton, P. D., "Preliminary Documentation of PAPST-Nonlinear Fracture and Analysis by Finite Elements", NSRDC - Preliminary Documentation, 1981.

[23] Washizu, K., Variational Methods in Elasticity and Plasticity, Pergamon Press, 1968.

[24] Hofmeister, D. L., Greenbaum, A. G. and Evensen, A. D., "Large Strain, Elasto-Plastic Finite Element Analysis", AIAA/ASME 11th Structures, Structural Dynamics and Materials Conference, Denver, 1970.

[25] Kachanov, L. M., Foundations of the Theory of Plasticity, North Hollow Pub. Co., 1971.

[26] Hill, R. H., The Mathematical Theory of Plasticity, Oxford University Press, 1950.

[27] Hilton, P. D. and Gifford, L. N., DTNSRDC-79/052/, Naval Ship Research Development Center Report, Bethesda, Maryland, 1979.

[28] Soete, W. and Denys, R., "The Development of a New Technique to Determine the Mechanical Properties in Butt Welds", Revue de la Soudure-Lastijdschrift, 4, Brussels, 1975.

[29] Gray, T. G. F., Spence, J. and North, T. H., Rational Welding Design, Butterworth and Company, Ltd., 1975.

[30] Munse, W. H., Vol. IV of Fracture, edit-d by H. Liebowitz, Academic Press, New York, pp. 382, 1969.

[31] Welding Handbook (Fundamentals of Welding) I, edited by A. L. Phillips, Published by American Welding Society, 1968.

VITA

Erdogan Madenci was born on August 1, 1958 in Ankara, Turkey to Halil and Zehra Madenci. He grew up in Ankara and graduated from Ankara Ataturk Lycée in June 1976.

As the second highest ranking student in nationwide examination, the author was awarded a full scholarship to persue his Bachelor and Master degrees in the United States. From November 1976 to December 1977, he studied English at George Washington and Georgetown Universities in Washington, D.C.

Mr. Madenci entered Lehigh University in January 1978. He received a Bachelor of Science degree in Mechanics in January 1981 and a Bachelor of Science in Industrial Engineering in October 1981, and was on the Dean's List several semesters. As a graduate student, Mr. Madenci worked as a research assistant with the Institute of Fracture and Solid Mechanics at Lehigh University.

The author is married to the former Diane M. Lindquist of Brockton, Massachusetts.